





**DISCOVERY OF NEW DUAL CATION AMMINE  
BOROHYDRIDES: A COMPUTATIONAL SCREENING STUDY**



**M.Sc. THESIS**

**Samet DEMIR**

**Computational Science and Engineering Department**

**Computational Science and Engineering Master Programme**

**MAY 2016**



**DISCOVERY OF NEW DUAL CATION AMMINE  
BOROHYDRIDES: A COMPUTATIONAL SCREENING STUDY**

**M.Sc. THESIS**

**Samet DEMİR  
(702131009)**

**Computational Science and Engineering Department**

**Computational Science and Engineering Master Programme**

**Thesis Advisor: Assoc. Prof. Adem TEKİN**

**Co-advisor: Dr. Suha Tuna**

**MAY 2016**



**İSTANBUL TEKNİK ÜNİVERSİTESİ ★ BİLİŞİM ENSTİTÜSÜ**

**YENİ İKİ METALLİ AMİN BOR HİDRÜRLERİN HESAPLAMALI TASARIMI:  
BİR HESAPSAL TARAMA ÇALIŞMASI**

**YÜKSEK LİSANS TEZİ**

**Samet DEMİR  
(702131009)**

**Hesaplamalı Bilim ve Mühendislik Anabilim Dalı**

**Hesaplamalı Bilim ve Mühendislik Yüksek Lisans Programı**

**Tez Danışmanı: Assoc. Prof. Adem TEKİN  
Eş Danışman: Dr. Suha Tuna**

**MAYIS 2016**





Samet DEMİR, a M.Sc. student of ITU Informatics Institute Engineering and Technology 702131009 successfully defended the thesis entitled “DISCOVERY OF NEW DUAL CATION AMMINE BOROHYDRIDES: A COMPUTATIONAL SCREENING STUDY”, which he/she prepared after fulfilling the requirements specified in the associated legislations, before the jury whose signatures are below.

**Thesis Advisor :**      **Assoc. Prof. Adem TEKİN** .....  
Istanbul Technical University

**Co-advisor :**          **Dr. Suha Tuna** .....  
Istanbul Technical University

**Jury Members :**      **Assoc. Prof. Adem TEKİN** .....  
Istanbul Technical University

**Assoc. Prof. Aylin SUNGUR** .....  
Istanbul Technical University

**Assoc. Prof. Şaron ÇATAK** .....  
Bogazici University

**Assoc. Prof. Şaron ÇATAK** .....  
Bogazici University

**Assoc. Prof. Şaron ÇATAK** .....  
Bogazici University

**Date of Submission :**    **2 May 2016**

**Date of Defense :**      **10 June 2016**





*To my lovely nephews; Zehra, Toprak and Neva,*



## **FOREWORD**

I would like to thank my advisor Assoc. Prof. Adem TEKİN for his invaluable suggestions, encouragements and guidance in writing the thesis and giving me the opportunity to work in the project.

I am also thankful to my friends, especially Gözde, Ahmet and Süha, for their support and help during the writing period.

Finally i would like to express my deepest gratitude to my family for supporting me everyway they can throughout my life.

May 2016

Samet DEMİR



## TABLE OF CONTENTS

	<u>Page</u>
<b>FOREWORD</b> .....	<b>ix</b>
<b>TABLE OF CONTENTS</b> .....	<b>xi</b>
<b>ABBREVIATIONS</b> .....	<b>xiii</b>
<b>LIST OF TABLES</b> .....	<b>xv</b>
<b>LIST OF FIGURES</b> .....	<b>xvii</b>
<b>SUMMARY</b> .....	<b>xix</b>
<b>ÖZET</b> .....	<b>xxi</b>
<b>1. INTRODUCTION</b> .....	<b>1</b>
1.1 Purpose of Thesis .....	3
1.2 Literature Review .....	3
1.3 Method.....	5
<b>2. METHODOLOGY</b> .....	<b>9</b>
2.1 Schrödinger Equation .....	9
2.2 Density Functional Theory .....	10
<b>3. RESULTS AND DISCUSSIONS</b> .....	<b>13</b>
3.1 Finding Model Structures .....	13
3.1.1 Crystal structure predictions for $M_1M_2(BH_4)_4(NH_3)_2$ .....	13
3.1.2 Crystal structure predictions for $M_1M_2(BH_4)_4(NH_3)_3$ .....	16
3.1.3 Crystal structure predictions for $M_1M_2(BH_4)_4(NH_3)_4$ .....	19
3.1.4 Crystal structure predictions for $M_1M_2(BH_4)_4(NH_3)_5$ .....	21
3.1.5 Crystal structure predictions for $M_1M_2(BH_4)_4(NH_3)_6$ .....	24
3.2 Computational Screening .....	25
3.2.1 Screening results for $M_1M_2(BH_4)_4(NH_3)_y$ .....	30
3.3 Conclusions .....	34
<b>REFERENCES</b> .....	<b>37</b>
<b>CURRICULUM VITAE</b> .....	<b>43</b>





## **ABBREVIATIONS**

<b>AMB</b>	: Ammine Metal Borohydride
<b>DFT</b>	: Density Functional Theory
<b>CASPESA</b>	: Crystal Structure Prediction via Simulated Annealin
<b>HF</b>	: Hartree-Fock
<b>GGA</b>	: Generalized Gradient Approximation
<b>CSP</b>	: Crystal Structure Prediction





## LIST OF TABLES

	<u>Page</u>
<b>Table 3.1</b> : Cell parameters of structures which are used in the screening. ....	29





## LIST OF FIGURES

	<u>Page</u>
<b>Figure 1.1</b> : Trigonal bipyramidal structure of $Mg(BH_4)_3(NH_3)_2$ from two different angle. Mg: green, B: pink, N: blue, H: white. ....	6
<b>Figure 1.2</b> : The model used in CASPESA. Li atoms are presented with purple balls. ....	7
<b>Figure 3.1</b> : Two different coordination around $M_2$ metal atom of $M_1M_2(BH_4)_4(NH_3)_2$ .....	13
<b>Figure 3.2</b> : $M_1M_2(BH_4)_4(NH_3)_2$ structures found by CASPESA.....	15
<b>Figure 3.3</b> : Three different coordinations around $M_2$ metal atom of $M_1M_2(BH_4)_4(NH_3)_3$ .....	16
<b>Figure 3.4</b> : $M_1M_2(BH_4)_4(NH_3)_3$ structures found by CASPESA.....	18
<b>Figure 3.5</b> : Two different coordination around $M_2$ metal atom of $M_1M_2(BH_4)_4(NH_3)_4$ .....	19
<b>Figure 3.6</b> : $M_1M_2(BH_4)_4(NH_3)_4$ structures found by CASPESA.....	21
<b>Figure 3.7</b> : Eight different coordinations around $M_2$ metal atom of $M_1M_2(BH_4)_4(NH_3)_5$ .....	22
<b>Figure 3.8</b> : $M_1M_2(BH_4)_4(NH_3)_5$ structures found by CASPESA.....	23
<b>Figure 3.9</b> : Three different coordinations around $M_2$ metal atom of $M_1M_2(BH_4)_4(NH_3)_6$ .....	24
<b>Figure 3.10</b> : $M_1M_2(BH_4)_4(NH_3)_6$ structures found by CASPESA.....	25
<b>Figure 3.11</b> : The alloying energy, $\Delta E_{alloy1}$ , as function of the decomposition energy, $\Delta E_{decomp1}$ . Representative colors: Li (Red), Na (Blue), K (Green). $NH_3$ content: x=2 (circle), x=3 (triangle), x=4 (square), x=5 (diamond) and x=6 (pentagon). ....	30
<b>Figure 3.12</b> : The alloying energy, $\Delta E_{alloy1}$ , as function of the decomposition energy, $\Delta E_{decomp2}$ . Representative colors: Li (Red), Na (Blue), K (Green). $NH_3$ content: x=2 (circle), x=3 (triangle), x=4 (square), x=5 (diamond) and x=6 (pentagon). ....	31
<b>Figure 3.13</b> : Hydrogen capacity (wt %) as a function of the decomposition energy, $\Delta E_{decomp1}$ . Representative colors: Li (Red), Na (Blue), K (Green). $NH_3$ content: x=2 (circle), x=3 (triangle), x=4 (square), x=5 (diamond) and x=6 (pentagon). ....	32
<b>Figure 3.14</b> : Hydrogen capacity (wt %) as a function of the decomposition energy, $\Delta E_{decomp2}$ . Representative colors: Li (Red), Na (Blue), K (Green). $NH_3$ content: x=2 (circle), x=3 (triangle), x=4 (square), x=5 (diamond) and x=6 (pentagon). ....	33
<b>Figure 3.15</b> : The decomposition energy, $\Delta E_{alloy1}$ , as a function of the average Pauling electronegativity. Representative colors: Li (Red), Na (Blue), K (Green). $NH_3$ content: x=2 (circle), x=3 (triangle), x=4 (square), x=5 (diamond) and x=6 (pentagon). ....	34



## **DISCOVERY OF NEW DUAL CATION AMMINE BOROHYDRIDES: A COMPUTATIONAL SCREENING STUDY**

### **SUMMARY**

Hydrogen is one of the promising alternatives for the replacement of fossil-fuels. One of the major bottlenecks preventing its widespread commercialization for on-board applications is to find the most suitable storage medium. Metal borohydrides are one of the classes of solid materials studied intensively to store hydrogen due to their high theoretical hydrogen capacities. However, their high thermodynamic stability is one of the major problems limiting their widespread usage. The requirement of high decomposition temperature can be lowered by the inclusion of ammonia. The resulting new complex containing both borohydrides and amines is called as Ammine Metal Borohydrides (AMBs). However, some of the AMBs have insuppressible release of ammonia during the dehydrogenation. This can be solved by the inclusion of a second metal atom into AMBs leading to dual-cation AMBs with a general formula of  $M_1M_2(BH_4)_x(NH_3)_y$ ,  $x=3-5$  and  $y=2-6$ . Until now, there are only a few synthesized dual cation AMBs reported in the literature. Therefore, by conducting a computational screening study we aim to find new AMBs with desired properties. In this respect, M1 was selected as an alkali metal (Li, Na or K) and M2 was assumed to be one of the following species: Mg, Ca, Ni, Mn, Sr, Zn, Al, Y, Sc, Ti, Zr and Co. The ideal case in a screening study is to use known crystal structures of the studied system. However, this is not an easy task and in general our target is to design new materials which are not seen on the literature. Therefore, employment of template structures is a well accepted strategy in such screening studies. A template structure refers that it is a prototype structure designed using the properties one of the system among the scope of the study. This template structure can be used for the other systems by just doing the proper replacements. For example, if a template structure generated for a system including Mg atom and the same structure can be invoked for a system including Zn by replacing Mg with Zn. Similar to the general situation depicted above, there is very limited information about the crystal structures of AMBs in the literature. Therefore, we found first template structures using a crystal structure prediction algorithm called as CASPESA. Subsequently, these structures were further relaxed at the DFT level. AMBs were evaluated with the help of some alloying and decomposition reactions. The results obtained so far indicate that many new AMBs were quite promising.

This work is a good example showing how supercomputers can be utilized to design new materials. In this case, the target is an energy material, however, the scope of design can easily be broadened e.g. to batteries or gas sensing materials. All these computational efforts allow a fast, economic and less expensive (in terms of time compared to experiment) way of strategy in both chemical and physical sciences.





## YENİ İKİ METALLİ AMİN BOR HİDRÜRLERİN HESAPLAMALI TASARIMI: BİR HESAPSAL TARAMA ÇALIŞMASI

### ÖZET

Alternatif enerji kaynağı arayışı günümüzde oldukça önemli bir çalışma konusudur. Bu çalışma alanının en büyük motivasyon kaynağı ise dünyanın artan enerji ihtiyacı ve popülasyonu ile birlikte, şu an geniş alanlarda enerji ihtiyacımızı karşılamakta olan fosil yakıtların tükenmeye başlamasıdır. Smil, V. 'nin [1] çalışmasına göre dünyanın yıllık enerji tüketimi 1860 yılında  $5 * 10^{12}$  kWsaat/yıl iken 2000 yılına gelindiğinde bu tüketim  $1.2 * 10^{14}$  kWsaat/yıl seviyesine yükselmiştir. Son bir yüzyılda insan popülasyonunun 4 kat arttığı göz önünde bulundurulursa, yıllık enerji tüketimindeki bu 24 kat artış hayli dikkate değerdir. British Petroleum'un 2007 yılında sağladığı verilere göre şu anda halihazırda bulunmuş olan fosil yakıt rezervlerimizin 40 yıl içinde tükeneceği öngörülmektedir. Bu sebeple fosil yakıtların yerini alacak olan materyalin yenilenebilir bir enerji kaynağı olması önemlidir. Alternatif enerji kaynağı arayışının bir başka önemli motivasyon kaynağı ise fosil yakıtların çevreye olan yıkıcı etkileridir. Son zamanlarda dünya azalan güneş etkinliği periyodundadır. Bu bilgiyle birlikte ortaya çıkan beklenti dünyanın ortalama sıcaklığının da azalmasıdır fakat aksine dünyanın ortalama sıcaklığı yıldan yıla artmaktadır ve bu duruma sebep olan en büyük faktör olarak fosil yakıt kullanımına bağlı oluşan sera gazlarıdır. Bu veriler ışığında kolayca söylenebilir ki; fosil yakıtlar olabildiğince kısa bir süre içinde daha uygun koşullar sağlayan bir enerji kaynağına yerini bırakmalıdır.

Hidrojen kütlece yüksek enerji yoğunluğu, yenilenebilir olması, dünyada bol miktarda bulunması ve çevre dostu karakteriyle fosil yakıtlar için iyi bir alternatif enerji kaynağıdır fakat aynı zamanda hidrojenin uygun enerji kaynağı olarak kullanılabilen duruma getirilebilmesi için çözülmesi gerek bazı problemleri de vardır. Bu problemlerden en önemlisi hidrojenin güvenli ve yüksek verimli depolanmasıdır. Hidrojen üretimi de kolay değildir, küçük hidrojen molekülleri depolanmak için oldukça kararsızlardır. Ayrıca şu anda kullanılan yakıt hücreleri platinyum gibi pahalı metaller kullanmakta ve bu da yüksek maliyete yol açmaktadır.

Hidrojen katı sıvı ve gaz formlarda depolanabilir fakat sıvı ve gaz depolamanın yüksek basınç gereksinimi veya hidrojen bozunumu için kriyojenik sıcaklık ihtiyacı gibi pratik kullanım için gerekli yaklaşımlara ters düşen ihtiyaçları onları katı depolama karşısında dezavantajlı hale getirmektedir. Örnekler vermek gerekirse, konvansiyonel çelik yapıları yüksek basınç tankları 20 MPa basınca kadar hidrojen depolama kapasitesine sahiptirler fakat artan basınçla birlikte tankın duvar kalınlığının da artması gerekliliği gravimetrik hidrojen depolama kapasitesini sınırlamaktadır. Hafif yapıları kompozit silindirelerle dayanılabilir basınç 80 MPa'ya kadar çıkartılabilir ve en yüksek verimlilikte  $40 \text{ kg } H_2/m^3$  miktarında hidrojen depolanabilir. Yüksek basınçta depolama tehlikeli sonuçlar doğurabilir. Bu yöntemin bir diğer zayıflığı

ise görece düşük depolama kapasitesidir. [2, 3] Sıvı halde hidrojen depolamak için kriyojenik tanklar kullanılabilir. Kriyojenik tankların hacimsel depolama kapasitesi  $40 \text{ kg H}_2/\text{m}^3$  miktarına kadar ulaşabilir ve bu miktar çelik yapılu yüksek basınç tanklarının depolama kapasitesinden fazladır. Kriyojenik tankların zayıf yönleri olarak ise sıvılaştırılmış nitrojen gibi ek malzemelere ihtiyaç duymaları ve hidrojen buharlaşması gösterilebilir. [3] Katı hidrojen depolama ise metal hidritler [4], karbon nanotüpler [5], metal-organik sistemler [6], metal borhidritler [7, 8], amonyum boran [9] ve amid/imid sistemleri [10] ile yapılabilir. Katı depolama materyalleri arasından metal borhidrürler ve metal aminler yüksek hidrojen depolama kapasiteleriyle ilgi uyandırmışlardır. Metal bor hidrürler için hidrojen depolama kapasitesi  $18.3 \text{ wt } \%$  miktarına kadar metal aminler için  $14.9 \text{ wt } \%$  miktarına kadar ulaşabilmektedir. Borhidrürlerin termodinamik olarak oldukça stabil olmaları, yani hidrojen salınımı için yüksek sıcaklıklara ihtiyaç duymaları, onları yaygın kullanım için kullanışsız duruma getirmektedir. [11, 12] Geçiş metalli bor hidrürler de metal bor hidrürler ve metal aminlere kıyasla daha iyi termodinamik özellikleriyle dikkat çekmektedirler fakat kararsız ve ortam sıcaklığında terisindir olmayan yapıları depolama malzemesi olarak kullanılmasının önündeki önemli problemlerdir. [7] Ayrıca amonyak da fosil yakıtlara alternatif bir enerji kaynağı olarak kullanılabilir. Amonyak karbonsuz yapısıyla yukarıda belirtilen hidrojen depolama yöntemlerine iyi bir rakip olarak düşünülebilir. Amonyak doğal gaz veya kömür vasıtasıyla üretilebilir. Günümüzde hayli gelişmiş amonyak üretim altyapıları ile amonyak üretimi sırasında  $\text{CO}_2$  salınımı baskılanabilmektedir. Tahmini olarak kömür rezervlerimizin 200 yıl içinde biteceğinin ön görülmesi ve amonyağın toksik bir materyal olması amonyağın enerji kaynağı olarak kullanılmasının önündeki engellerdir. Yapılan yeni bir çalışma ki;  $\text{Al}(\text{BH}_4)_3$  ile  $\text{NH}_3$  koordine edilerek,  $\text{Al}(\text{BH}_4)_3(\text{NH}_3)_6$  oluşturularak, stabilize edilebileceğini göstermiştir. [13] Bu yaklaşım diğer metal borhidrürlere genişletilebilir. Metal bor hidrürlere  $\text{NH}_3$  eklenmesiyle oluşturulan bu yeni tür materyallere amin metal borhidrürler (AMB) denir. Tek katyonlu AMB'leri genel formülü  $\text{M}(\text{BH}_4)_m(\text{NH}_3)_n$  ( $\text{M} = \text{Li, Mg, Ca, Al, Zn vb.}$ ) şeklindedir. Tek katyonlu AMB'lerin ana problemleri olarak hidrojen salınımı sırasında yakıt hücrelerini zehirleyen amonyağın ortaya çıkması ve yüksek salınım sıcaklığı göstermeleridir. (örnek olarak  $\text{Ca}(\text{BH}_4)_2(\text{NH}_3)_2$  [14] ve  $\text{LiBH}_4 \cdot \text{NH}_3$  [15]) Şu anda literatürde AMBlerle ilgili çok sayıda çalışma olmasa da, var olan çalışmalar bu materyallerin gelecek için fazlasıyla umut vaat ettiğini göstermektedir. Yapılan çalışmalar gösteriyor ki; tek katyonlu AMBlerin zayıf yönleri bileşiğe ikinci bir katyon eklenmesiyle, yani çift katyonlu amin metal bor hidrür oluşturulmasıyla, giderilebilir.

Çift katyonlu AMBler hakkında teorik ve deneysel bilgiler henüz yeni bir çalışma alanı olduklarından dolayı oldukça kısıtlıdır. Ayrıca çift katyonlu amin metal bor hidrürler bu tezde irdelenen ana konudur ve genel formülü  $\text{M}_1\text{M}_2(\text{BH}_4)_4(\text{NH}_3)_x$ ,  $\text{M}_1 = \text{Li, Na, K}$ ,  $\text{M}_2 = \text{Al, Sc, Mo, Co, Y, Ti}$ ,  $x = 2,3,4,5,6$  olan çift katyonlu AMBler bu tezde incelenmiştir. Literatürde mevcut olan çift katyonlu AMBlere örnek olarak,  $\text{LiMg}(\text{BH}_4)_3(\text{NH}_3)_2$  [16],  $\text{NaZn}(\text{BH}_4)_3(\text{NH}_3)_2$  [17],  $\text{Li}_2\text{Mg}(\text{BH}_4)_5(\text{NH}_3)_6$  [18] gösterilebilir. Sentezlenmesi başarılı olmuş bu malzemelerin hepsi Amerikan Enerji Departmanının (DOE) hidrojen depolama malzemeleri için belirlediği kapasite hedefinin üzerinde bir depolama kapasitesine sahiptirler.

Bu çalışmada benzetilmiş tavlama (simulated annealing) algoritmasına dayalı bir kristal yapı tahmin yazılımı ve yoğunluk fonksiyonel teori (YFT) kullanılarak çift katyonlu AMBler için bir tarama yapılmıştır. Bu tarama sonucunda da çift katyonlu

AMBlerin alařım oluřturma ve bozunma enerjileri gz nnde bulundurularak hidrojen depolamaya en uygun materyaller tespit edilmeye alıřılmıřtır. Tezin konusu olan komplekslerin ok byk bir kısmının kristal yapı bilgileri mevcut deęildir. Kristal yapı bilgisi bir malzemenin fiziksel zellikleri ile doęrudan iliřkili olduęundan byk nem arz etmektedir. Eęer bir materyalin detaylı kristal yapı bilgisi biliniyorsa, materyal henz sentezlenmemiř dahi olsa o materyalin zellikleri ngrlebilmektedir. Bu sebeple alıřmanın ilk blmnde grubumuz tarafından geliřtirilen benzetilmiř tavlama algoritmasına dayalı kristal yapı tahmin programı olan CASPESA (CrystAl PrEdiction via Simulated Annealing) kullanılarak tezin konusu olan yukarıda bahsedilen malzemelerin kristal yapısı tahmin edildi. CASPESA daha nce metal borhidrr arařtırmalarında [19–23] ve ayrıca metal amin arařtırmalarında [24, 25] bařarıyla uygulanmıřtır. Her bileřiğin birden fazla olası kristal yapısı olduęundan, bu ihtimallerin her biri iin CASPESA ayrı ayrı uygulanmıřtır. CASPESA tarafından yapılan bu alıřma erevesinde toplamda bir milyona yakın kristal yapı tahmini yapılmıřtır. Bu yapıların arasından depolama aısından en umut vaadedeęi dřnlenleri bulmak iin yine grubumuz tarafından geliřtirilen bir sonuları sınıflandırma yazılımı kullanılmıřtır. Bu iřlemin ardından umut verici olarak bulunan yapıların yoęunluk fonksiyonel teorisi ile atomik koordinatları ve aę rgs parametreleri eniyilenmiřtir.

Tarama alıřması yapılan materyaller arasında Al ile birlikte Li ieren materyaller en yksek hidrojen ierięine sahip materyallerdir. Ayrıca Li ile birlikte Sc ve Ti ve Na ile birlikte Al ieren yapılar da olduka yksek hidrojen ierięine sahiptirler. Taranan yapılar arasında deneysel olarak halihazırda sentezlenmiř tek yapı olan  $\text{LiSc}(\text{BH}_4)_4(\text{NH}_3)_4$  hedeflenen blgede bulunmuřtur. Tarama alıřmasında materyallerin bozunma ve alařım oluřturma incelendięinde sonu olarak Mo (Li, Na, K ile birlikte), Co (Li, Na, K ile birlikte ve  $x < 6$  iken, ayrıca  $\text{NaCo}(\text{BH}_4)_4(\text{NH}_3)_4$  hari), Ti (Li, Na, K ile birlikte,  $\text{NaTi}(\text{BH}_4)_4(\text{NH}_3)_4$  hari) ve Al (Li, Na, K ile birlikte ve  $x < 5$  iken) gelecek vaadeden materyaller olarak belirlenmiřtir. Tarama iřlemi yapılan materyallerden sadece bir tanesinin sentezlenmiř olduęu gz nne alındıęında, bu alıřma sonucunda deneysel olarak sentezlenebilecek gelecek vaadeden daha bir ok çift katyonlu AMBnin olduęu gsterilmiřtir.



## 1. INTRODUCTION

With the growing energy need of the world and the population, our fuel supplies, which is mostly depended on fossil fuels, started to run out. According to Smil, V. [1] our energy consumption per year was  $5 * 10^{12} kWh/year$  in the year of 1860 and in 2000 it is increased to  $1.2 * 10^{14} kWh/year$ . It means while human population increases by a factor of 4 in the last century, energy consumption increased by 24 and based on British Petroleum's 2007 data current fossil fuel reserves will run out within 40 year. This situation force researchers to search for new energy sources. Another motivation of these research activities are due to the harmful effects of fossil fuels on health and the environment. Currently the earth is in decreased solar activity period, this indicates that average temperature of the earth should decrease but instead average temperature is increasing. The biggest reason of this situation is the increased emission of greenhouse gases which is caused by usage of fossil fuels. In the light of these informations one can easily conclude that fossil fuel must be replaced by a both environment friendly and renewable source. Hydrogen can be a great replacement for fossil fuels with its environment friendly nature, high energy content and renewability however there is some major difficulties which must be surmounted before using hydrogen as a energy carrier. The biggest technical problems for the implementation of hydrogen as an energy carrier are the safety and the efficient way of storage. On the other hand, hydrogen production is also not an easy task in addition to the challenges faced in fuel cell applications due to the requirement of expensive catalysts like platinum. Hydrogen can be stored as in the form of gas, liquid or solid but gas and liquid forms require very high pressure and cryogenic temperatures, respectively, to decompose hydrogen which is not convenient for use of hydrogen in the on-board applications. Conventional steel based high-pressure tanks are capable of storing hydrogen gas at pressures up to 20 MPa but the wall thickness of the tank has to be increased with the pressure and this limits the gravimetric storage capacity. To overcome this problem light weight composite cylinders are developed which can resist the pressures up to 80 MPa and their storing capacity, at maximum, is  $40 kg H_2/m^3$ . [3]. Storage

with high pressures are dangerous and this is the major problem of the high pressure tanks alongside with low storage capacity [2, 3]. Cryogenic tanks can be used for storing hydrogen in liquid form. Volumetric hydrogen capacity of cryogenic tanks can reach up to  $40 \text{ kg H}_2/\text{m}^3$  and this capacity is higher than high-pressure tanks. Cryogenic tanks need liquefied nitrogen and this is an extra cost. Also another disadvantage of cryogenic tanks is permanent boil-off of the hydrogen [3]. Storing hydrogen in solid materials can be accomplished with metal hydrides [4], carbon nanotubes [5], metal-organic frameworks [6], metal borohydrides [7, 8], ammonia boranes and amides. The criteria concerning the suitable storage material are having high hydrogen storage capacity, applicable thermodynamics and fast hydriding and dehydriding kinetics. Among the solid storage materials metal borohydrides and metal amines have attracted uttermost interest because of their gravimetric capacities, for metal borohydrides  $18.3 \text{ wt } \%$  and for metal amines it is  $14.9 \text{ wt } \%$ . Problem of metal borohydrides is they are thermodynamically too stable (AT makale 3-4), so to release hydrogen they need very high temperatures which makes them out of favour for widespread use. Also transition metal borohydrides attract some attentions with their better thermodynamic properties when we compare them with the metal borohydrides, however they are unstable or irreversible at ambient temperatures [7]. Furthermore ammonia can be another alternative to fossil fuels. It is carbon-free and it has high hydrogen density which makes it a challenger to hydrogen storage methods which mentioned above. Ammonia can be produced from natural gas or coal. Current ammonia infrastructures are very advanced and can suppress  $\text{CO}_2$  release while production. Still we have to keep in mind that calculated expiration of coal reserves is about 200 years from now. Also ammonia is a toxic material and that makes it displeasing. A new study showed that  $\text{Al}(\text{BH}_4)_3$  can be stabilized by coordinating it with  $\text{NH}_3$ , forming  $\text{Al}(\text{BH}_4)_3(\text{NH}_3)_6$  [13]. This approach can be expanded to other metal borohydrides. With the addition of  $\text{NH}_3$  to metal borohydrides, new types of materials so called ammine metal borohydrides (AMBs) [14, 15, 26–32] can be formed. The general formula of these mono-cation AMBs are  $\text{M}(\text{BH}_4)_m(\text{NH}_3)_n$  ( $\text{M} = \text{Li, Mg, Ca, Al, Zn}$  and etc.). The metal type used in the AMBs influence the proximity of hydrogen atoms in B-H and N-H groups and causes dihydrogen bonds formation. AMBs need lower temperature for dehydrogenation when we compare them with the metal borohydrides. The key problem with AMBs is the undesired release of ammonia

during the hydrogenation which poison the fuel cell and leading to high desorption temperature. (e.g  $\text{Ca}(\text{BH}_4)_2(\text{NH}_3)_2$  [14] and  $\text{LiBH}_4 \cdot \text{NH}_3$  [15])

## 1.1 Purpose of Thesis

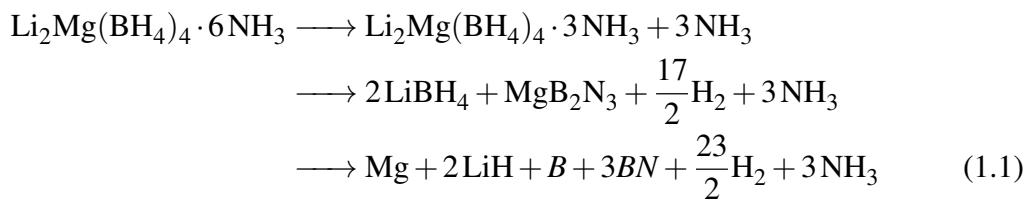
There is not much studies present concerning AMBs at the literature currently. On the other hand prior few studies showed that with adding a second metal atom to AMBs, forming dual-cation AMB, can improve the favourableness of AMBs to use them as hydrogen storage materials. In this study dual-cation AMBs which has the general formula of  $\text{M}_1\text{M}_2(\text{BH}_4)_4(\text{NH}_3)_x$  where  $\text{M}_1 = \text{Li, Na, K}$ ,  $\text{M}_2 = \text{Al, Sc, Mo, Co, Y, Ti}$ ,  $x = 2, 3, 4, 5, 6$  were investigated. This study covers predictions of crystal structures, Density Functional Theory (DFT) calculations to design new storage materials based on dual cation AMBs. With the help of this screening, we will have a chance to find a material showing better storage capabilities. Ultimately, such new compounds might lead to new experimental studies.

## 1.2 Literature Review

AMBs with two cations are fresh research area and there is an increasing interest to dual cation AMBs due to their promising features.. Therefore, there is only a few reports in the literature. Guo et al. [27] had synthesized  $\text{Al}(\text{BH}_4)_3(\text{NH}_3)_x - y\text{LiBH}_4$  ( $x < 6$  and  $y < 3$ ) and showed that the storage characteristics of AMBs can be improved with the addition of a second cation. While  $\text{Al}(\text{BH}_4)_3 \cdot 4\text{NH}_3$  has a hydrogen capacity of 15.5 wt %,  $\text{Al}(\text{BH}_4)_3 \cdot 4\text{NH}_3 - \text{LiBH}_4$  has 16.1 wt % hydrogen with enhanced thermodynamics. It is also noteworthy that unwanted ammonia during the dehydrogenation can be surpassed by changing ammonia content in the system. In the another recent study carried out by Sun et al. [16]  $\text{LiMg}(\text{BH}_4)_3(\text{NH}_3)_2$  was synthesized. They reported that the material is capable of releasing 8 % wt hydrogen below 200 °C They synthesized this material by ball milling of  $\text{Mg}(\text{BH}_4)_2$  and  $\text{LiBH}_4 \cdot \text{NH}_3$ . Furthermore, In their study, they have observed emission peaks at 388.5°C which might be due to  $\text{LiBH}_4$  decomposition. Decomposition temperature of pure  $\text{LiBH}_4$  is 480°C, hence one can consider that coaction between  $\text{LiMg}(\text{BH}_4)_3(\text{NH}_3)_2$  and  $\text{LiBH}_4$  can be the reason of this lowered decomposition temperature.  $\text{Ca}(\text{BH}_4)_2(\text{NH}_3)_2$  was synthesized by Chu et al. [33].

They observed in their research that  $\text{Ca}(\text{BH}_4)_2(\text{NH}_3)_2$  can release 11.3 % *w* of its hydrogen below  $250^\circ\text{C}$ . When we compare this value with decomposition temperature and hydrogen content of  $\text{Ca}(\text{BH}_4)_2$ , which are  $500^\circ\text{C}$  and 9 % *w* respectively, it can easily be seen that forming AMBs can cause positive achievements. Furthermore another mono-cation AMB,  $\text{Mg}(\text{BH}_4)_2(\text{NH}_3)_2$ , which contains 16 % *w* hydrogen was synthesized by Soloveichik et al. [28]. This mono-cation AMB starts releasing hydrogen at  $120^\circ\text{C}$  and can release % 12 of its hydrogen content under  $250^\circ\text{C}$ . When we compare these values with the ones obtained for  $\text{Mg}(\text{BH}_4)_2$ , which starts releasing hydrogen at  $250^\circ\text{C}$  and release approximately % 12 of its hydrogen content at  $400^\circ\text{C}$ , we can observe the improvement in the properties brought by AMBs. Another synthesized mono-cation AMB is  $\text{Y}(\text{BH}_4)_3(\text{NH}_3)_4$  which was synthesized by Yuan et al. [30]. This material can release % 8.7 of its hydrogen at  $250^\circ\text{C}$  while  $\text{Y}(\text{BH}_4)_3$  can only release % 3.2 at the same temperature. Another recent dual-cation AMB,  $\text{NaZn}(\text{BH}_4)_3(\text{NH}_3)_2$ . was synthesized by Xia et al. [17]. They found that this material can release % 7.9 of its hydrogen content at  $110^\circ\text{C}$  without releasing unwanted ammonia or diaborane gasses.  $\text{Li}_2\text{Mg}(\text{BH}_4)_5(\text{NH}_3)_6$  was synthesized by Guo et al. [18]. They observed that  $\text{Li}_2\text{Mg}(\text{BH}_4)_5(\text{NH}_3)_6$  is releasing % 10 of its hydrogen below  $120^\circ\text{C}$  with a very high purity above % 99.

Decomposition reactions of AMBs are not easy to predict, since they follow a wide range of complex routes. It has been reported by Yang et al. [34] that  $\text{Li}_2\text{Mg}(\text{BH}_4)_4(\text{NH}_3)_6$  decomposes following the reactions shown below:



The results obtained so far in the literature indicate that both of mono- and dual-cation ambms have superior hydrogen storage properties compared to metal borohydrides. Therefore, it is wise to consult new research activities to explore new AMBs. In this particular study, we made a computational screening of dual cation AMBs with a general formula of  $\text{M}_1\text{M}_2(\text{BH}_4)_4(\text{NH}_3)_x$  where  $x = 2, 3, 4, 5, 6$  and a classification,



based on experimental works we have mentioned above, to find which dual cation AMBs are more suitable for hydrogen storage.

### 1.3 Method

The crystal structure details of AMBs are very limited in the literature. In order to design new AMBs, we require their crystal structures. In such cases, crystal structure prediction plays a vital role by providing a crystal structure. With this motivation our research group had developed an algorithm based on simulated annealing, called CrystAl Structure PrEdiction via Simulated Annealing (CASPEsa), to predict crystal structures of materials. In this thesis, the crystal structures of  $M_1M_2(BH_4)_4(NH_3)_x$ , where  $M_1 = Li, Na, K$ ,  $M_2 = Al, Sc, Mo, Co, Y, Ti$ ,  $x = 2, 3, 4, 5, 6$ , were predicted with CASPEsa. CASPEsa was successfully used for various materials before such as metal amines [24, 25] and metal borohydrides [19–23]. To understand how CASPEsa works and how we implement CASPEsa for dual-cation AMBs, a constructive example would be useful. For this purpose,  $LiMg(BH_4)_3(NH_3)_2$  material was selected and explained below in detail. CASPEsa is still in the production step and there is no an automatic way to employ it for any system yet. Caspesa requires a carefully selected initial parameter set (bond distances) for a better performance. While modelling dual-cation AMBs, for each ammonia content a different optimization setup has been employed. For example, a free  $BH_4$  group appears only in some certain cases where additional parameters must be introduced. Thus, the structural details were carefully adjusted for each system under consideration. The bond constraints are first extracted from the literature if there is any available data. If there is nothing found in the literature, DFT calculations can be performed using the structures optimized with CASPEsa together with imperfect constraints. Then, the structural details obtained from the DFT structure can be subsequently employed in the production run of CASPEsa. Actually, our group already implemented this idea, in thesis of Engin Aybey, and it has been shown that such a strategy is really working for  $Mn(BH_4)_2$  and  $LiMg(BH_4)_3(NH_3)_2$ . Thus, CASPEsa can be run for any system even if there is no information in the literature. However, switching on DFT calculations, generally around for 10 different structures, creates a need of fast supercomputers. In this implementation, the algorithm continues until there is no any further change in the

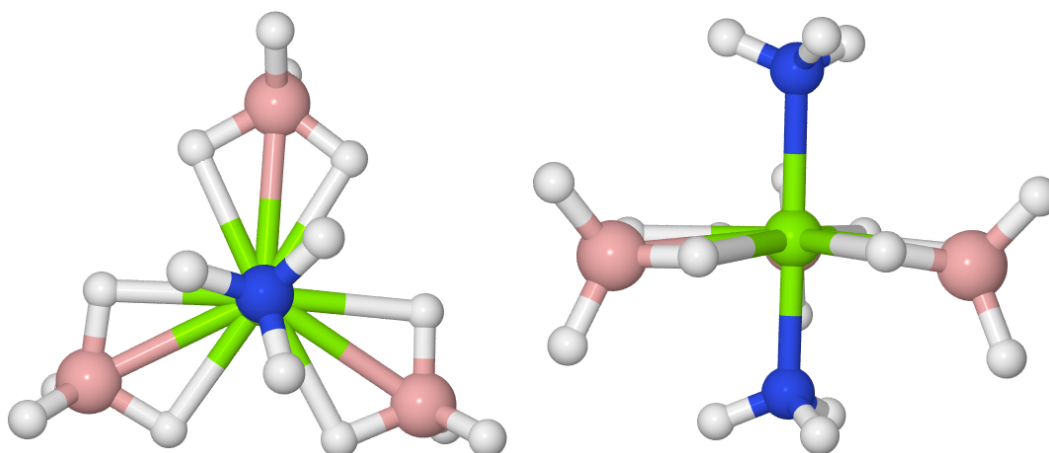


**Figure 1.1** : Trigonal bipyramidal structure of  $\text{Mg}(\text{BH}_4)_3(\text{NH}_3)_2$  from two different angle. Mg: green, B: pink, N: blue, H: white.

energy computed with DFT. Then the bond constraints can be extracted from these structures and a final CASPESA run is invoked. It should also be mentioned that CASPESA performs a global optimization using simulated annealing approach. In any global optimization, an objective function is tried to be minimized. This objective function can be simply the energy of the system. In CASPESA, our objective function is the number of arrangements that should have potential to lower the energy. Hydrogen bonding is an example for such an arrangement. Preceding studies [16, 17] show that alkali metals in AMBs tend to bond with  $\text{BH}_4$  groups while alkaline earth metals or transition metals tend to bond with both  $\text{NH}_3$  and  $\text{BH}_4$  groups. Moreover, dihydrogen bonds between N-H and B-H groups affects the stability of dual cation AMBs. These two arrangements are employed as the objective function and they are maximized in CASPESA.

The setup of CASPESA is exemplified for  $\text{LiMg}(\text{BH}_4)_3(\text{NH}_3)_2$ , since a very similar system was employed in  $\text{M}_1\text{M}_2(\text{BH}_4)_4(\text{NH}_3)_{2-6}$ . Figure 1.1 shows the  $\text{Mg}(\text{BH}_4)_3(\text{NH}_3)_2$  group used in the unit cell. Here, three  $\text{BH}_4$  groups (at the equatorial positions) and two ammonias (at the axial positions) are coordinated in a trigonal bipyramidal fashion. Since such an arrangement is apparent in the experimental crystal structure of  $\text{LiMg}(\text{BH}_4)_3(\text{NH}_3)_2$  [16]. This group was also included as a whole rather than individual  $\text{BH}_4$  and ammonias. This trigonal bipyramid organization can move or rotate in the unit cell. Two formula units of  $\text{LiMg}(\text{BH}_4)_4(\text{NH}_3)_2$  were used in one unit cell as it can be seen in the figure 1.2. Li atom in the center has a fixed position at origin. Other Li atom and two  $\text{Mg}(\text{BH}_4)_3(\text{NH}_3)_2$  groups are able to change their

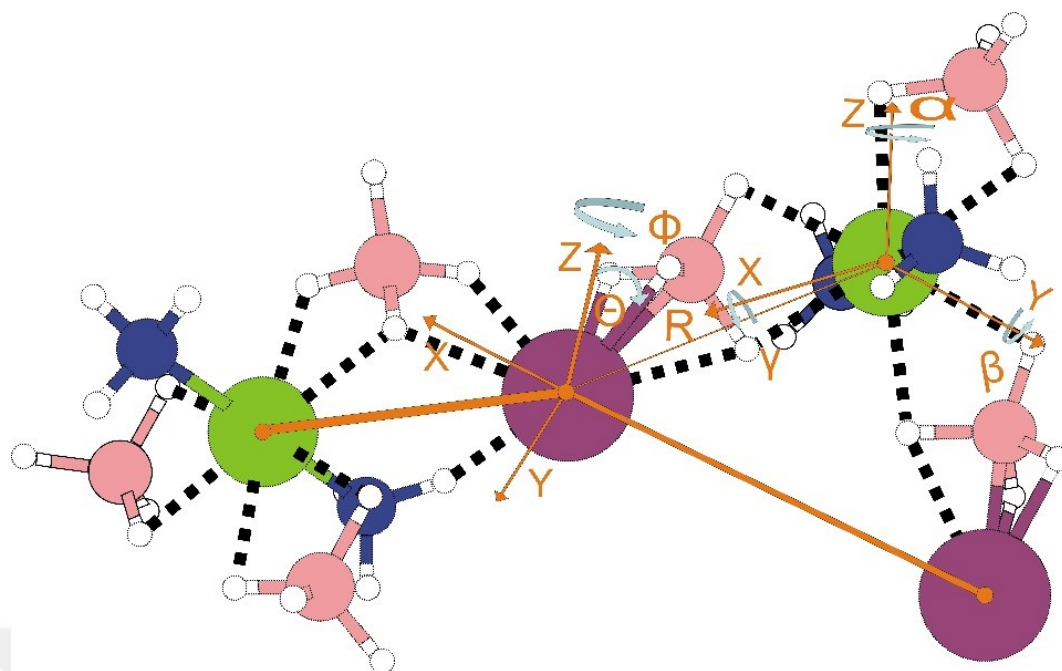


**Figure 1.2** : The model used in CASPESA. Li atoms are presented with purple balls.

positions. Also  $\text{Mg}(\text{BH}_4)_3(\text{NH}_3)_2$  has ability to rotate around its own center. In order to increase the objective function, the proper rotation and translation of these groups are allowed. There are 15 structural parameters in this unit cell. Among them, 9 of them are for movements of Li atom and  $\text{Mg}(\text{BH}_4)_3(\text{NH}_3)_2$  groups and the remaining ones are for the rotation of  $\text{Mg}(\text{BH}_4)_3(\text{NH}_3)_2$  groups. In addition to atomic positions, the shape of the unit cell was also parametrized. We require 1-9 (e.g., 1 for cubic and 9 for a triclinic cell) parameters for the unit cell and thus the total number of parameters varies in between 16-24.

Simulated annealing is a global optimization method but in CASPESA we used it for a maximization problem. As already indicated, interaction between  $\text{LiBH}_4$  and lithium was used in the objective function. Here, if the Li-B distance is in the following range, 2.85-3.31 Å, the value of the objective function is increased by 1. In CASPESA there is no quantum mechanical or a force field based computation is used, as a result atoms can take place too close to each other which leads to non-physical situations. To halt this behaviour some distance threshold as called before bond constraints must be introduced in the CASPESA. These limits were set based on findings of Sun et al. [16]. More specifically, the following maximum bonding distances were applied: Li-Li, Li-B, H-H, Li-N and N-N minimum inter-atomic distances were interpreted respectively as follows 4.0, 2.0, 1.6, 3.0 and 4.2 Å.

In this study, number of considered structure is 90(3 type of alkali metal (Li, Na, K), 6 type of transition metal (Al, Sc, Mo, Co, Y, Ti) and 5 different ammonia content (2,3,4,5,6)). For every structure, we used one or more models (average is 4). For each ammonia content, several different unit cell configurations (as an average of 4) were employed in CASPESA. Each CASPESA optimization was repeated at least 400 times leading to more than a million run in total.  $(3(\text{alkaline metals}) * 6(\text{transition metals}) * 5(\text{ammonia content}) * 4(\text{model amount}) * 7(\text{unit cell type}) * 400(\text{run amount}))$ . It is very hard to select the best structures to perform DFT computations, therefore an analysis script was prepared for the automatic evaluation of the structures. This tool searches for specific arrangements like the coordination around Li atoms and removes redundant structures. The best structures were further relaxed at the DFT level using Quantum Espresso suit [35]. PBE (Perdew, Burke, Ernzerhof) [36] generalized gradient approximation (GGA) exchange-correlation has been used and norm conserving pseudopotentials were included in the calculations. The kinetic energy and density cutoffs were set to 80 and 320 Ry. The energy and force thresholds were set to  $10^{-5}$  and  $10^{-4}$  a.u. respectively.

## 2. METHODOLOGY

### 2.1 Schrödinger Equation

The time dependent schrödinger equation of an isolated system with N electrons can be represented as below:

$$\hat{H}\Psi = E\Psi \quad (2.1)$$

Where H is the Hamiltonian operator,  $\Psi = \Psi(r_1, r_2, \dots, r_N)$  is the many body wave function and E is the electronic energy of the system. The Hamiltonian operator,  $\hat{H}$ , in atomic units can be expressed as:

$$\hat{H} = -\frac{1}{2} \sum_i^{electrons} \nabla_i^2 - \frac{1}{2} \sum_i^{nuclei} \frac{1}{M_A} \nabla_A^2 - \sum_i^{electrons} \sum_A^{nuclei} \frac{Z_A}{r_{iA}} + \sum_i^{electrons} \sum_{j>i}^{electrons} \frac{1}{r_{ij}} + \sum_A^{nuclei} \sum_{B>A}^{nuclei} \frac{Z_A Z_B}{R_{AB}} \quad (2.2)$$

Here, Z denotes the nuclear charge,  $M_A$  denotes the ratio of mass of nucleus A to the mass of an electron,  $R_{AB}$  is the distance between nucleus A and B,  $r_{ij}$  is the distance between electron i and j and finally  $r_{iA}$  is the distance between nucleus A and electron i.

$\Psi$  characterizes the state of the system. The many-electron Schrödinger equation is impossible to solve exactly even for simple systems, for instance hydrogen molecule or helium atom. Thus approximations can be used to solve it. One of the leading approximation to solve Schrödinger equation is Born-Oppenheimer approximation. It depends on assumption of ignoring the movement of the nuclei. Needless to say, nuclei do move but their movement speed is negligible when compared to movement speed of the electron, which is quite close to speed of the light. Born-Oppenheimer approximation assumes Schrödinger equation as:

$$\hat{H}^{el}\Psi^{el} = E^{el}\Psi^{el} \quad (2.3)$$

$$\hat{H}^{el} = -\frac{1}{2} \sum_i^{electrons} \nabla_i^2 - \sum_i^{electrons} \sum_A^{nuclei} \frac{Z_A}{r_{iA}} + \sum_i^{electrons} \sum_{j>i}^{electrons} \frac{1}{r_{ij}} \quad (2.4)$$

It can clearly be seen that  $\hat{H}$  has missing terms; nuclear kinetic energy and nuclear-nuclear Coulomb term. Born-Oppenheimer approximation considers nuclear kinetic energy to be zero and as a result it disappears. Other missing term, nuclear-nuclear Coulomb term, is a constant in Born-Oppenheimer approximation and it can be estimated as:

$$E^{nuc} = \sum_A^{nuclei} \sum_{B>A}^{nuclei} \frac{Z_A Z_B}{R_{AB}} \quad (2.5)$$

With using energy gathered from the simplified Schrödinger equation,  $E^{el}$ , and the correction from the nuclear energy, the total energy of a system can be calculated as:

$$E = E^{el} + E^{nuc} \quad (2.6)$$

Born-Oppenheimer approximation makes Schrödinger equation feasible by computers. After the approximation, leading approaches to solve the Schrödinger equation can be ordered as: i) Semi-Empirical methods which depends on experimental data ii) Ab-Initio methods which is based on calculated data iii) Density Functional Methods which is based on energy calculation on electron density.

## 2.2 Density Functional Theory

With the technological developments in capacity and power of computers, calculations on computers have become an essential tool for physics and chemistry. Empirical and semi-empirical methods have been around for fair amount of time but with the increasing processing power more demanding ab initio calculations became popular. Density Functional Theory(DFT), which is capable of giving the complete quantum mechanical description without having complexity of many-body Schrödinger equation, is one of the most popular method.

DFT is a method which uses electron density to calculate the ground state energy. This theory originated from a model which introduced by Llewellyn Thomas and Enrico Fermi in 1927. Thomas-Fermi model provides an expression, which depended on electron gas model, for the kinetic energy. This model is using only electron density and it only works in the limit of an infinite nuclear charge. Furthermore, the Hartree approximation introduced mean potential based on the electron density alone and also

Dirac, Slater and Gaspar had improved exchange potential models for electron gas and atoms. In the year of 1964, Hohenberg and Kohn [37] introduced two significant theorems based upon the ideas mentioned above. They showed that every stationary quantum mechanical observable, including energy, can be calculated precisely from the ground state electron density. Another prove they showed is that the calculated total energy for the trial density cannot be lower than the true ground state energy.

DFT offers higher accuracy with lower computation cost when compared to Hartree-Fock (HF) based methods. Besides DFT considers the interactions between electron pairs while HF methods does not. In DFT calculation of electronic energy contains sum of separately calculated terms:

$$E = E_T + E_V + E_J + E_{XC} \quad (2.7)$$

Here,  $E_T$  is the kinetic energy,  $E_V$  is the nucleus-nucleus attraction and nucleus-nucleus related potential energy,  $E_J$  is the potential energy from Coulomb energy and  $E_{XC}$  is the exchange correlation term.

All terms in the equation above, except nucleus-nucleus repulsion, can be written as function of electron density.  $E_{XC}$  can be separated into two functions; exchange and correlation. Since the exchange energy is a result of the antisymmetry of the quantum mechanical wave function, correlation energy is originated from correlation in the motions of individual electrons.

These terms, being functions of electron density, enable the previous equation to be rewritten as:

$$E[\rho] = \int v(r)\rho(r)dr + T[\rho] + V_{ee}[\rho] \quad (2.8)$$

above,  $v(r)$  is the potential energy,  $\rho$  is the electron density,  $T[\rho]$  is the kinetic energy and  $V_{ee}[\rho]$  is representing interelectronic interactions. When applied to Kohn-Sham approach to the last equation, it becomes:

$$E[\rho] = \int v(r)\rho(r)dr + T_s[\rho] + J(\rho) + E_{XC}[\rho] \quad (2.9)$$

Here,  $J[\rho]$  is Coulomb energy (electron-electron repulsion). Kohn-Sham approach utilizes  $T_s[\rho]$ : kinetic energy of non-interacting system of electrons.

$$T_s[\rho] = \sum_{i=1}^N \langle \Psi_i \left[ -\frac{1}{2} \nabla^2 \right] \Psi_i \rangle \quad (2.10)$$

$E_{XC}[\rho]$  ; exchange correlation functional:

$$E_{XC}[\rho] = T[\rho] - T_s[\rho] + V_{ee} - J[\rho] \quad (2.11)$$

Functional derivative of  $E_{XC}$  is  $v_{xc}$  and it can be calculated as:

$$v_{xc} = \frac{\partial E_{xc}[\rho]}{\partial(\rho)} \quad (2.12)$$

$E_{XC}$  can be written as sum of exchange functional and correlation functional:

$$E_{XC}[\rho] = E_X[\rho] + E_C[\rho] \quad (2.13)$$

After, in order to express the system of non-interacting electrons under an external effective potential, here denoted as  $v_{eff}(r)$ , following equation can be utilized:

$$v_{eff}(r) = v(r) + \frac{\partial J[\rho]}{\partial \rho(r)} + \frac{\partial E_{XC}[\rho]}{\partial \rho(r)} = v(r) + \int \frac{\rho(r')}{|r-r'|} dr' + v_{XC}(r) \quad (2.14)$$

Now, an equation similar to Schrödinger's have obtained:

$$\left[ -\frac{1}{2}\nabla^2 + v_{eff}(r) \right] \Psi_i = \varepsilon_i \Psi_i \quad (2.15)$$



### 3. RESULTS AND DISCUSSIONS

#### 3.1 Finding Model Structures

As detailed in the introduction section, this thesis is about finding suitable dual-cation AMBs for hydrogen storage. This dual-cation AMBs can be represented as  $M_1M_2(BH_4)_4(NH_3)_x$  where  $M_1 = Li, Na, K$ ,  $M_2 = Al, Sc, Mo, Co, Y, Ti$  and  $x = 2, 3, 4, 5, 6$ . There is very few information available in the literature about these materials. CASPESA were used to predict crystal structures of these materials. Then, the best structures obtained with CASPESA were further refined with DFT computations.

##### 3.1.1 Crystal structure predictions for $M_1M_2(BH_4)_4(NH_3)_2$

Two different coordinations as shown in Figure 3.1 were used to design the unitcell of  $M_1M_2(BH_4)_4(NH_3)_2$  in CASPESA.

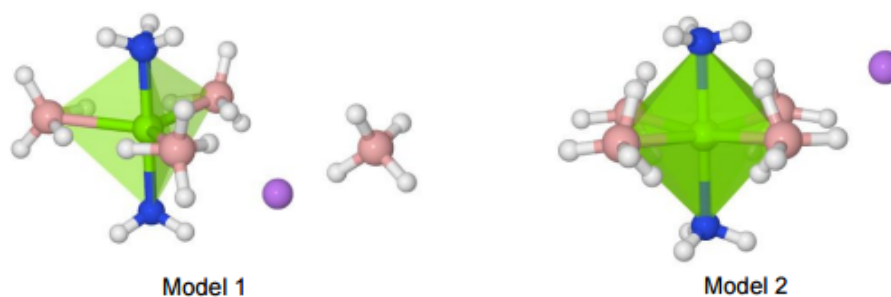
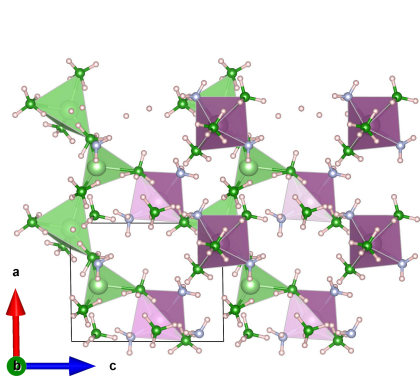


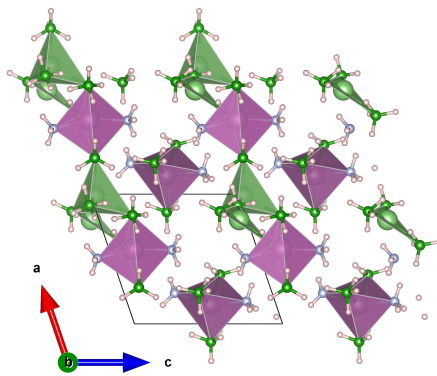
**Figure 3.1** : Two different coordination around  $M_2$  metal atom of  $M_1M_2(BH_4)_4(NH_3)_2$

Model1 is consists of a trigonal bipyramidal arrangement around  $M_2$  atom, which contains two  $NH_3$  groups located at the axial positions and three  $BH_4$  groups in the equatorial positions, with an additional mobile  $BH_4$  group. Model2 is made up from an octahedral coordination including two axial  $NH_3$  and four equatorial  $BH_4$  groups. Crystal structure predictions (CSP) were carried out using these two unitcell configurations with the help of CASPESA. After the CSPs, selected structures were

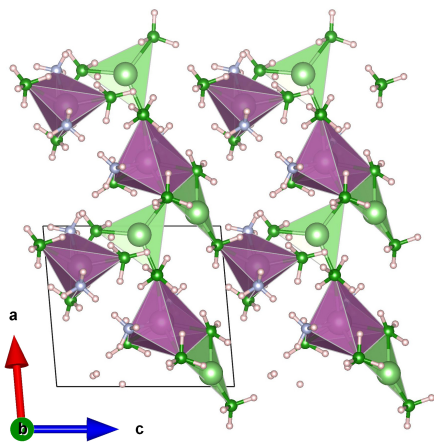
optimized by DFT calculations. The resulting optimized structures can be seen in figure 3.2.



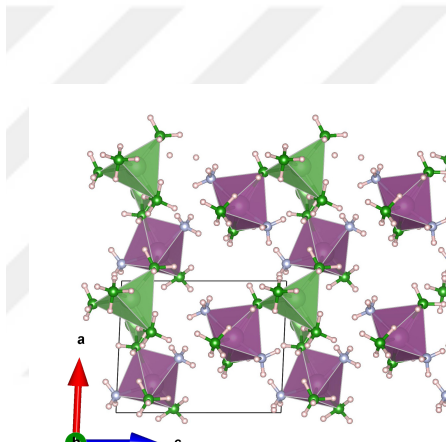
(a) B4N2\_1 (symmetry no: 1)



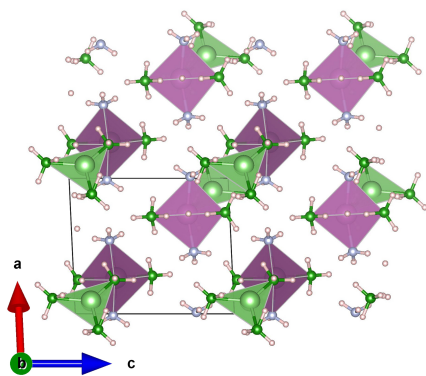
(b) B4N2\_2 (symmetry no: 1)



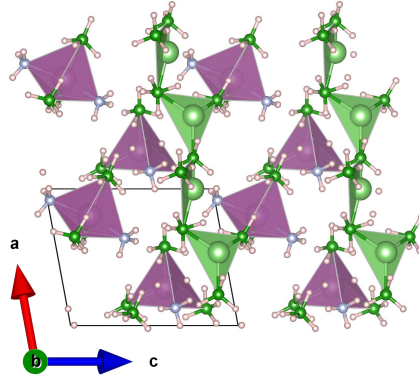
(c) B4N2\_3 (symmetry no: 1)



(d) B4N2\_4 (symmetry no: 1)



(e) B4N2\_5 (symmetry no: 2)



(f) B4N2\_6 (symmetry no: 1)

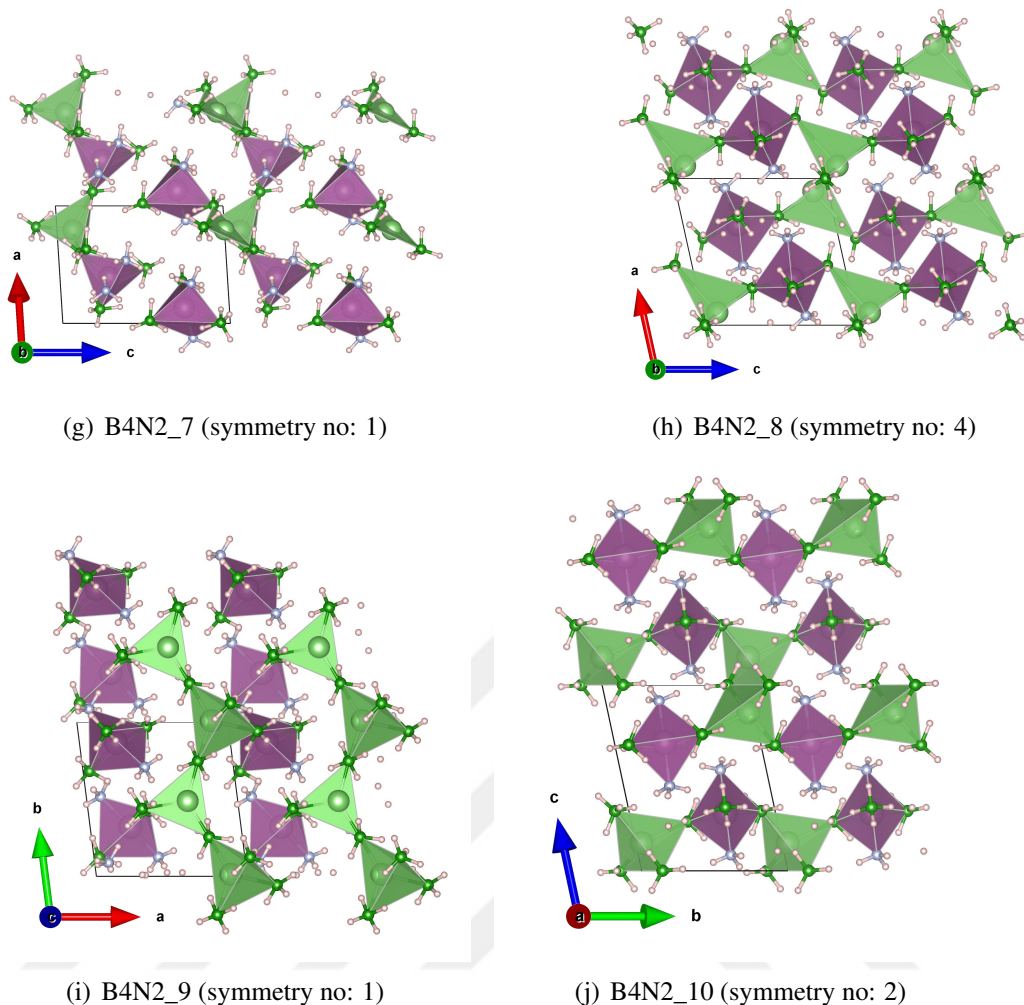


**Figure 3.2** :  $M_1M_2(BH_4)_4(NH_3)_2$  structures found by CASPESA

In B4N2\_1 structure, there is a trigonal bipyramidal arrangement around  $M_2$  metal containing three  $BH_4$  and two  $NH_3$  groups.  $M_1$  atoms are in coordination with  $BH_4$  groups in both trigonal and tetragonal arrangements.  $M_1$  atoms are constitutes a chain parallel to  $[100]$  plane with sharing one  $BH_4$  group and two  $M_1$  chains are connected to each other via the  $BH_4$  gorups bound to  $M_2$ . In B4N2\_2 coordinations around  $M_2$  metals are similar to B4N2\_1, however these two structure differ in  $M_1$  coordinations. While one  $M_1$  atom is in the trigonal coordination with  $BH_4$  groups, other  $M_1$  atom prefers a tetrahedral formation. These two groups form a chain parallel to  $[010]$  plane with sharing one  $BH_4$ . The tetrahedral and trigonal  $M_1$  groups share a  $BH_4$  group with trigonal bipyramidal  $M_2$ . As a consequence of this situation,  $M_2-Li$  distance is shortened up to  $4.2 \text{ \AA}$ . The main difference in B4N2\_3 from the previous structures is that all of the  $M_1$  atoms form a trigonal coordination with  $BH_4$  groups. One of the  $M_1$  group is connected to  $M_2$  group by sharing one  $BH_4$ . In the case of the other  $M_1$

group, they share one  $\text{BH}_4$  group from two different  $\text{M}_2$  groups. Thus, they created a chain parallel to  $[100]$  plane.  $\text{B4N2}_4$  is very similar to  $\text{B4N2}_2$ . In this structure, trigonal and tetrahedral  $\text{M}_1$  groups are connected to each other by sharing one  $\text{BH}_4$  group. In addition, they shared one  $\text{BH}_4$  group from  $\text{M}_2$  creating a chain. In  $\text{B4N2}_5$ , connections around  $\text{M}_2$  are similar to the previous structures and  $\text{M}_1$  groups have a trigonal coordination.  $\text{M}_1$  groups are connected to each other by sharing  $\text{BH}_4$  groups (Li - Li distance is 2.85 Å) and each  $\text{M}_1$  shares one  $\text{BH}_4$  with  $\text{M}_2$  but they did not create a chain. In  $\text{B4N2}_6$ , trigonal  $\text{M}_1$  groups share one of their  $\text{BH}_4$  with each other and create a chain parallel to  $[100]$  plane. Moreover, one of the  $\text{M}_1$  group is bound to  $\text{M}_2$  by sharing a  $\text{BH}_4$ . In structure  $\text{B4N2}_7$ ,  $\text{M}_1$  atoms have both trigonal and tetrahedral coordinations and share one of their  $\text{BH}_4$  molecule with  $\text{M}_2$  groups. In structure  $\text{B4N2}_8$ , trigonally coordinated  $\text{M}_1$  groups constitute a chain parallel to  $[010]$  plane.  $\text{B4N2}_9$  is quite similar to  $\text{B4N2}_8$  with a difference that one of the  $\text{M}_1$  prefers a tetrahedral. In  $\text{B4N2}_{10}$  structure, all  $\text{M}_1$  atoms are in the tetrahedral coordination and they share one of their  $\text{BH}_4$  molecule with  $\text{M}_2$  metal constituting a chain parallel to  $[010]$  plane.

### 3.1.2 Crystal structure predictions for $\text{M}_1\text{M}_2(\text{BH}_4)_4(\text{NH}_3)_3$

Three models shown in figure 3.3 were employed in CASPESA.

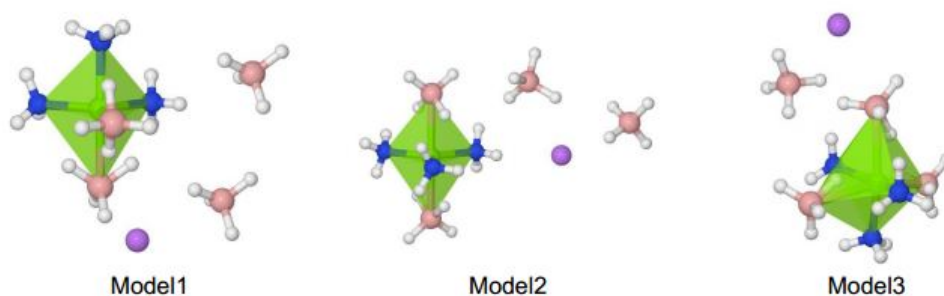
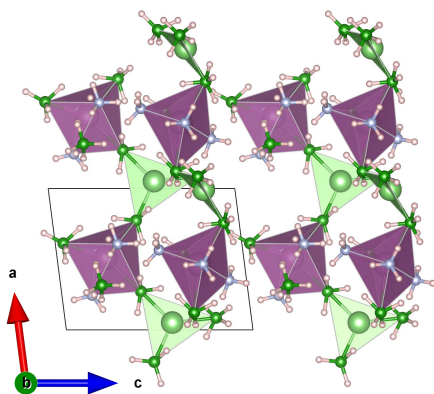


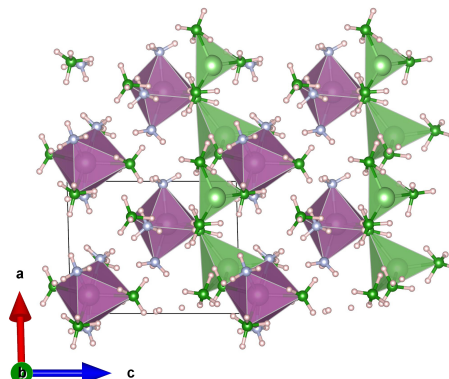
**Figure 3.3** : Three different coordinations around  $\text{M}_2$  metal atom of  $\text{M}_1\text{M}_2(\text{BH}_4)_4(\text{NH}_3)_3$

In Model1,  $\text{M}_2$  metal has a trigonal bipyramidal coordination with three  $\text{NH}_3$  and two  $\text{BH}_4$  groups. Model2 is similar to Model1 but in Model2  $\text{BH}_4$  and  $\text{NH}_3$  groups have a different bonding preferences (while  $\text{BH}_4$  groups are located in the axial positions,  $\text{NH}_3$  groups are in the equatorial positions). In addition, this two models contain two free  $\text{BH}_4$  groups. In the case of Model3, there are three  $\text{BH}_4$  and  $\text{NH}_3$  groups connected

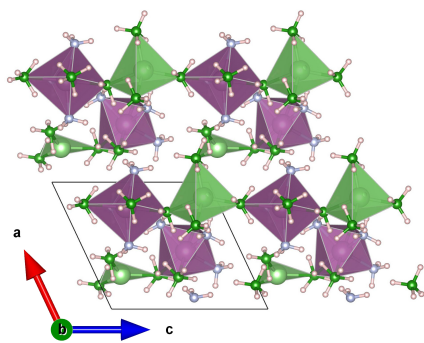
to  $M_2$  octahedrally. This model also contains a free  $BH_4$  group. The template structures obtained from these models are shown in figure 3.4.



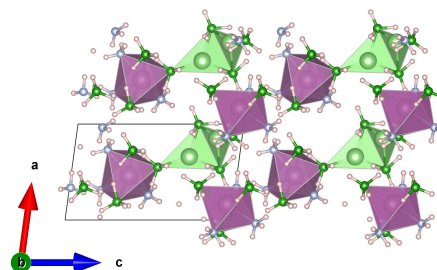
(a) B4N3\_1 (symmetry no: 1)



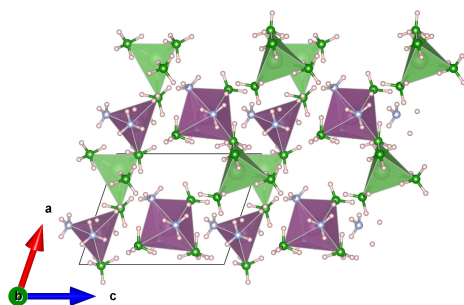
(b) B4N3\_2 (symmetry no: 1)



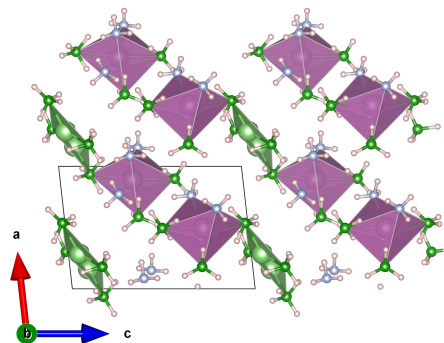
(c) B4N3\_3 (symmetry no: 1)



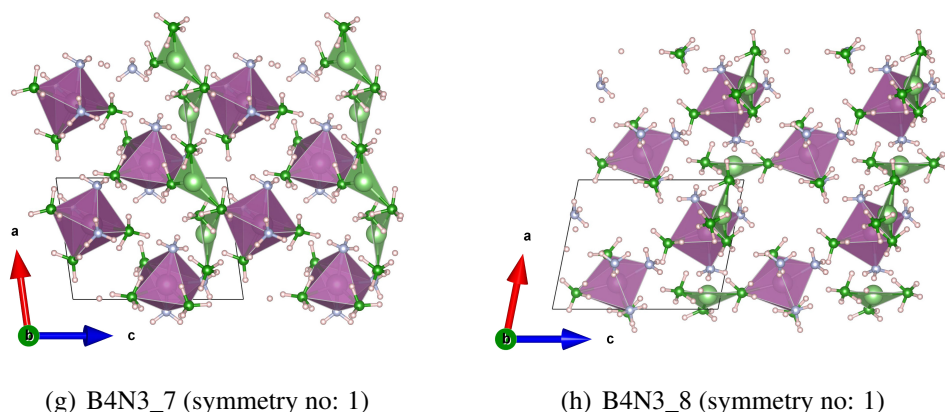
(d) B4N3\_4 (symmetry no: 1)



(e) B4N3\_5 (symmetry no: 1)



(f) B4N3\_6 (symmetry no: 1)



(g) B4N3\_7 (symmetry no: 1)

(h) B4N3\_8 (symmetry no: 1)

**Figure 3.4** :  $M_1M_2(BH_4)_4(NH_3)_3$  structures found by CASPESA

In structure B4N3\_1, there is an octahedral coordination around  $M_2$  formed by three  $BH_4$  and  $NH_3$  groups. All  $M_1$  atoms in this structure are in the trigonal coordination and form a chain parallel to  $[100]$  plane together with  $M_2$  by sharing a  $BH_4$  group. B4N3\_2 is similar to B4N3\_1 but in this structure  $M_1$  atoms form also a tetrahedral coordination in addition to the trigonal one. In the tetrahedral and trigonal coordinations,  $M_1$  atoms also share one  $BH_4$  molecule with each other. Moreover,  $M_1$  atoms also creates a chain with  $M_2$  metal by sharing a  $BH_4$ . B4N3\_3 is quite similar to B4N3\_2 and it has a chain parallel to  $[001]$  plane. This chain can be represented as  $Li-M_2-Li-M_2$ . The difference in B4N3\_4 from the other structures is that there is a trigonal bipyramidal organization around  $M_2$  metal in addition to an octahedral geometry. This trigonal bipyramidal geometry is formed by three  $NH_3$  and two  $BH_4$  groups. All  $M_1$  atoms forms a trigonal geometry and share their two  $BH_4$  groups with each other. One of the  $M_1$  atom shares two  $BH_4$  groups with the octahedrally coordinated  $M_2$  metal. Trigonal bipyramidal formed by  $M_1$  atoms does not lead to any chain.  $M_2$  in B4N3\_5 has both trigonal bipyramidal and octahedral coordinations similar to B4N3\_4. All  $M_1$  atoms in this structure are in a tetrahedral coordination. Some of the  $M_1$  metal atoms shares their two  $BH_4$  groups with the others. Furthermore,  $M_1$  atoms create a chain parallel to  $[100]$  plane with  $M_2$  groups by sharing one  $BH_4$  group. In structure B4N3\_6, while all  $M_2$  atoms are in an octahedral coordination,  $M_1$  atoms prefers a tetrahedral bonding. Besides,  $M_1$  atoms form a chain parallel to  $[010]$  direction by sharing one  $BH_4$  group. Although B4N3\_7 is quite similar to B4N3\_6, it contains an additional trigonal bipyramidal coordination around  $M_2$  metal. In this structure, trigonal  $M_1$  atoms are located parallel to  $[100]$  plane. The last

template structure of  $M_1M_2(BH_4)_4(NH_3)_3$  is B4N3\_8 and it only contains octahedral and trigonal coordinations around  $M_2$  and  $M_1$  respectively. Two of the  $M_1$  groups share one  $BH_4$  molecule with each other and they connected to  $M_2$  groups by sharing one  $BH_4$  molecule.

### 3.1.3 Crystal structure predictions for $M_1M_2(BH_4)_4(NH_3)_4$

Two different models shown in figure 3.5 were used to study  $M_1M_2(BH_4)_4(NH_3)_4$  by CASPESA.

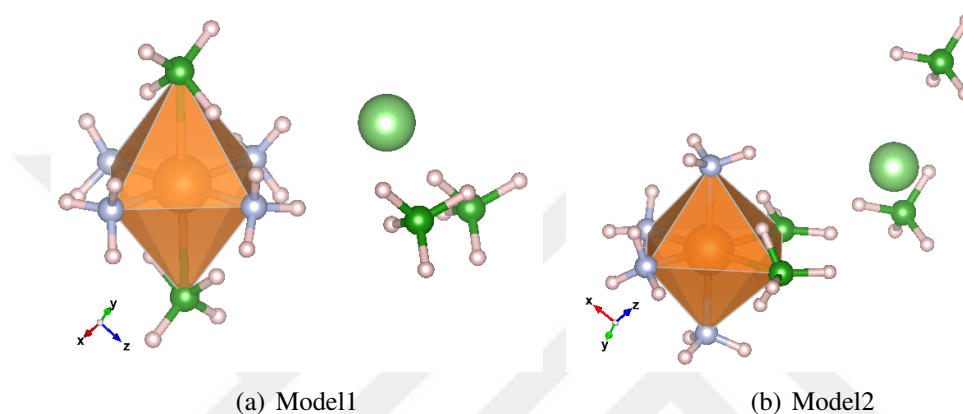
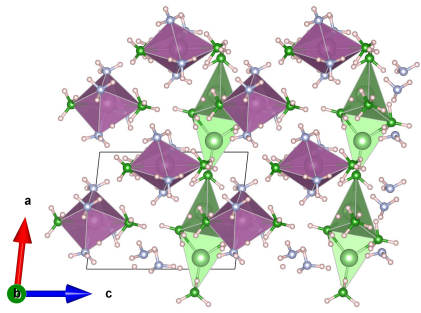
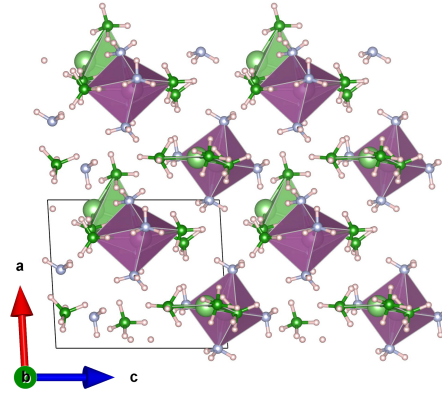


**Figure 3.5** : Two different coordination around  $M_2$  metal atom of  $M_1M_2(BH_4)_4(NH_3)_4$

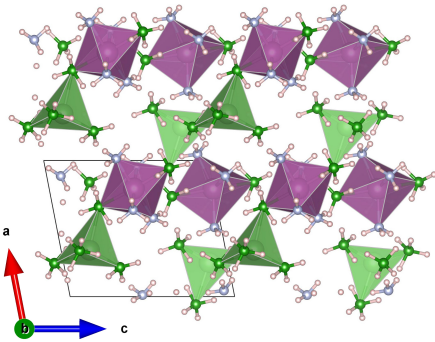
Both of them are in an octahedral coordination with four  $NH_3$  and two  $BH_4$  groups around  $M_2$ . While all  $NH_3$  groups are in the equatorial positions in Model1, two of them are in axial two of them are in equatorial positions in Model2. These models also have two mobile  $BH_4$  groups. The template structures obtained from these models are shown in figure 3.6.



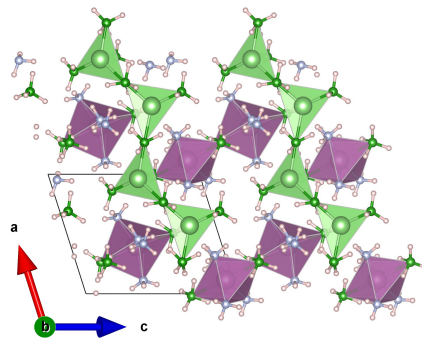
(a) B4N4\_1 (symmetry no: 1)



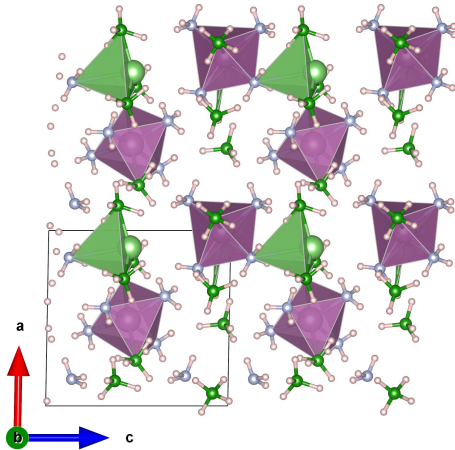
(b) B4N4\_2 (symmetry no: 1)



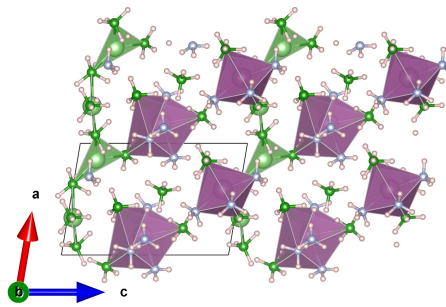
(c) B4N4\_3 (symmetry no: 1)



(d) B4N4\_4 (symmetry no: 1)

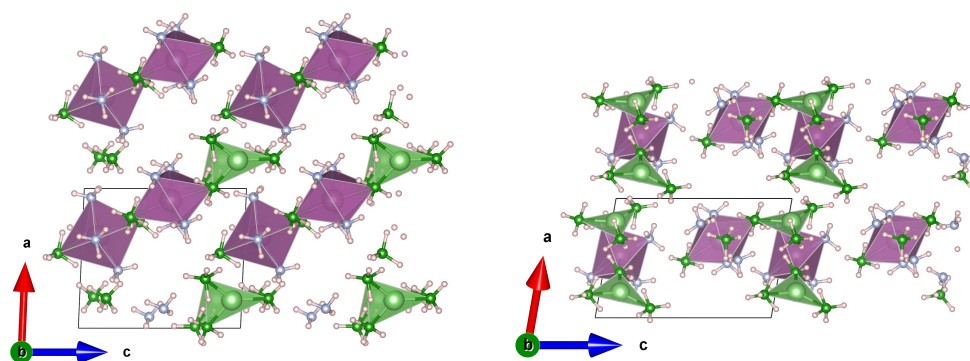


(e) B4N4\_5 (symmetry no: 1)



(f) B4N4\_6 (symmetry no: 1)





(g) B4N4\_7 (symmetry no: 1)

(h) B4N4\_8 (symmetry no: 1)

**Figure 3.6** :  $M_1M_2(BH_4)_4(NH_3)_4$  structures found by CASPESA

The first model is B4N4\_1 and it has an octahedral coordination formed by three  $BH_4$  and  $NH_3$  groups around  $M_2$ . All  $M_1$  atoms are in a trigonal formation with  $BH_4$  groups.  $M_2$  and  $M_1$  groups are create a chain parallel to [100] plane by sharing one  $BH_4$  group. Coordinations around  $M_2$  metal in B4N4\_2 are similar to that of B4N4\_1 with an additional tetrahedral coordinations. Trigonal and tetrahedral arrangements formed around  $M_1$  are connected to each other by sharing a  $BH_4$  group. Moreover,  $M_1$  and  $M_2$  metals create a chain by sharing a  $BH_4$  group. B4N4\_3 is very similar to B4N4\_2 with a difference of chain formation parallel to [001] direction by  $M_1$  and  $M_2$  metals. B4N4\_4 contains a trigonal bipyramidal arrangement in addition to an octahedral one. This trigonal bipyramidal coordination formed around  $M_2$  contains three  $NH_3$  and two  $BH_4$  group.  $M_1$  atoms only form trigonal geometry in this template. They are also connected to each other by sharing two of their  $BH_4$  groups. Furthermore, one of the  $M_1$  atom is connected to an octahedral  $M_2$  by sharing a  $BH_4$ . The trigonal bipyramidal  $M_2$  does not lead to any chain formation. B4N4\_5 is very similar to B4N4\_2. In this structure  $M_2$  and  $M_1$  atoms create a chain parallel to [010] plane by sharing a  $BH_4$  group. In B4N4\_6 structure,  $M_2$  atoms form both octahedral and trigonal prism arrangements.  $M_1$  atoms create a chain parallel to [100] plane by sharing a  $BH_4$  group. In B4N4\_7, all  $M_2$  metals form an octahedral coordination, while all  $M_1$  metals constitute trigonal bonding with  $BH_4$  groups. The last template for  $M_1M_2(BH_4)_4(NH_3)_4$  is B4N4\_8 and the coordinations are quite similar to B4N4\_7.

### 3.1.4 Crystal structure predictions for $M_1M_2(BH_4)_4(NH_3)_5$

Eight different models shown in figure 3.7 were used in crystal structure prediction of  $M_1M_2(BH_4)_4(NH_3)_5$ .

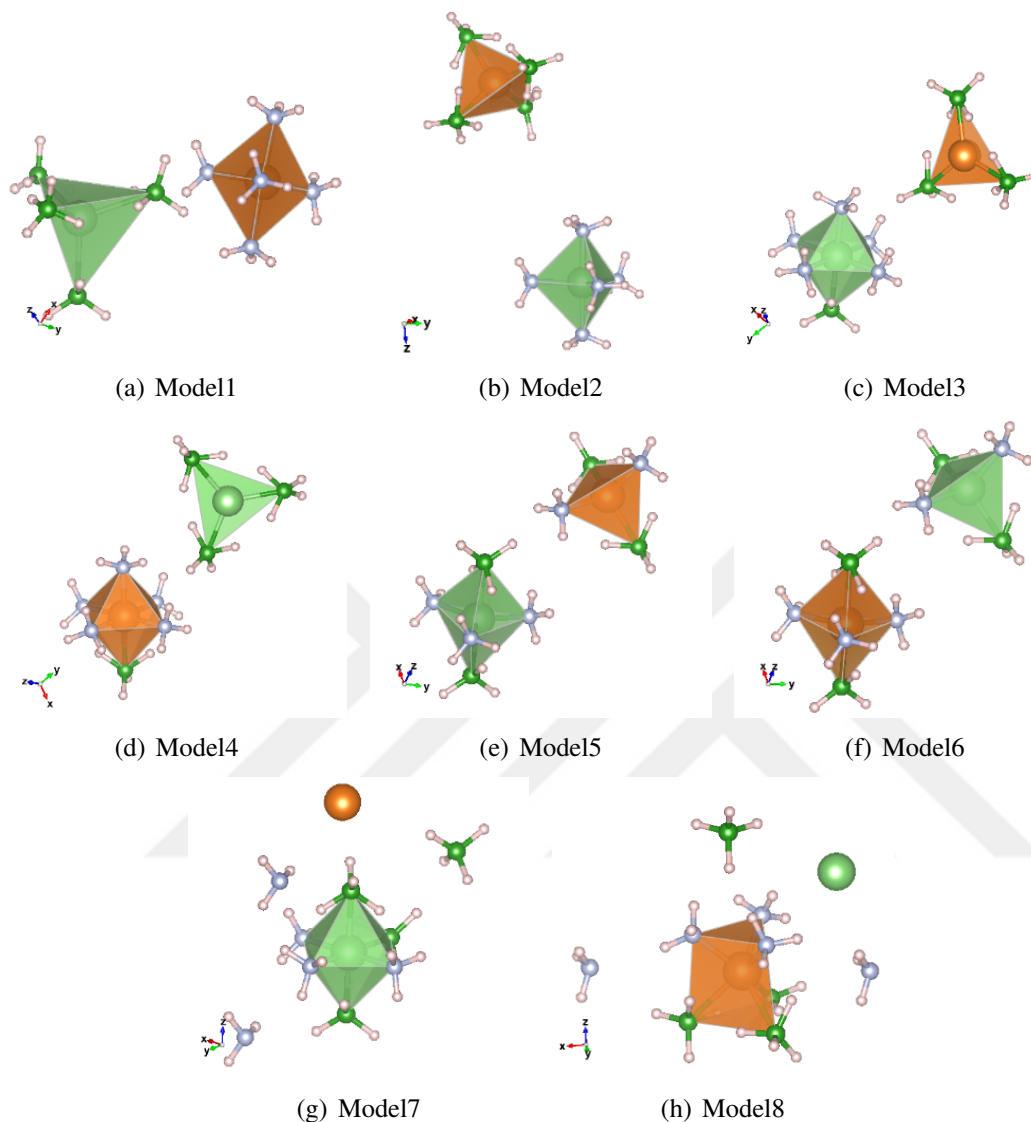


**Figure 3.7 :** Eight different coordinations around  $M_2$  metal atom of  $M_1M_2(BH_4)_4(NH_3)_5$

The first model, Model1, contains both tetrahedral and trigonal bipyramidal coordinations. In particular,  $M_1$  prefers a tetrahedral arrangement Tetrahedral geometry formed by a  $M_1$  atom and four  $BH_4$  group while trigonal bipyramidal geometry formed by a  $M_2$  atom and five  $NH_3$  group. Model2 differs from Model1 by the preference of metal atoms coordination (their positions were swapped). In Model3, while  $M_1$  metal forms an octahedral arrangement with five  $NH_3$  and one  $BH_4$ ,  $M_2$  prefers a trigonal coordination with three  $BH_4$  groups. Model4 is swapped metal version of Model3. Model5 contains both a trigonal bipyramidal and tetrahedral

arrangements. There is a trigonal coordination consisting of three  $\text{NH}_3$  and two  $\text{BH}_4$  groups around  $\text{M}_1$ . On the other hand, a tetrahedral arrangement is present around  $\text{M}_2$  containing two  $\text{NH}_3$  and  $\text{BH}_4$  groups. Model6 is a swapped metal atom version of Model5. Up to now, there is no mobile  $\text{BH}_4$  or  $\text{NH}_3$  groups present in the considered models. Model7 and Model8 contain also mobile  $\text{BH}_4$  and  $\text{NH}_3$  groups. In Model7, there is an octahedral coordination consisting of three  $\text{NH}_3$  and  $\text{BH}_4$  groups around  $\text{M}_1$ . The last model, Model8, includes a trigonal prism with three  $\text{BH}_4$  and  $\text{NH}_3$  groups around  $\text{M}_2$ .

As shown in the figure 3.8 three template structures were obtained with the help of these 8 models.

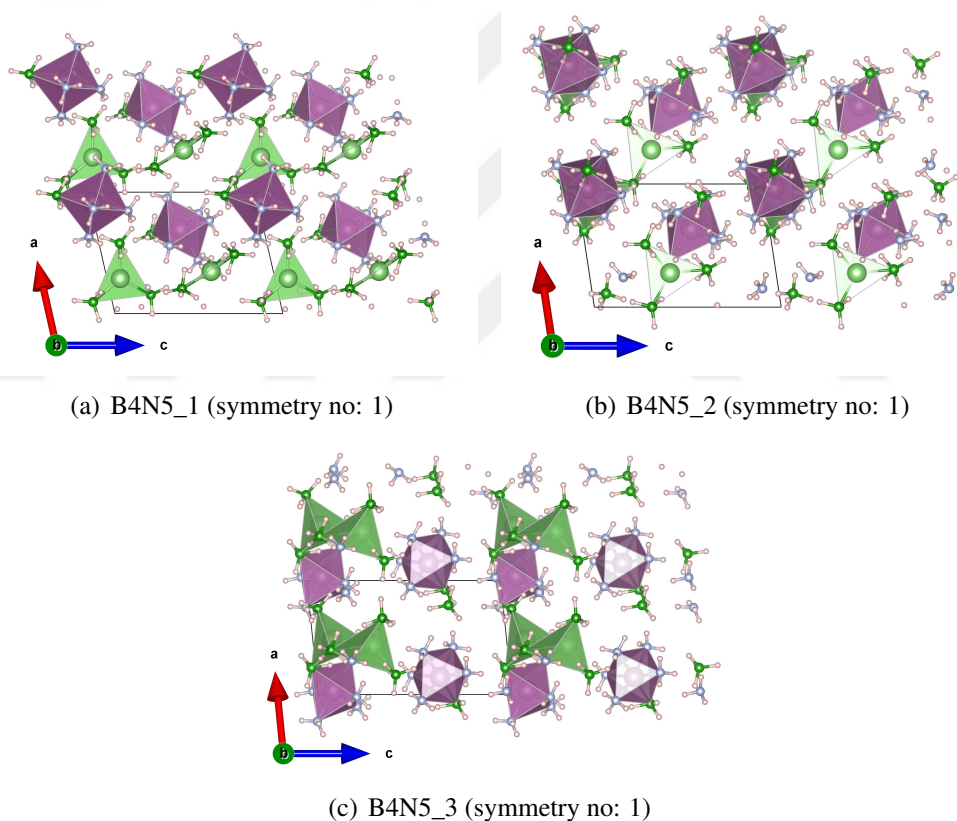


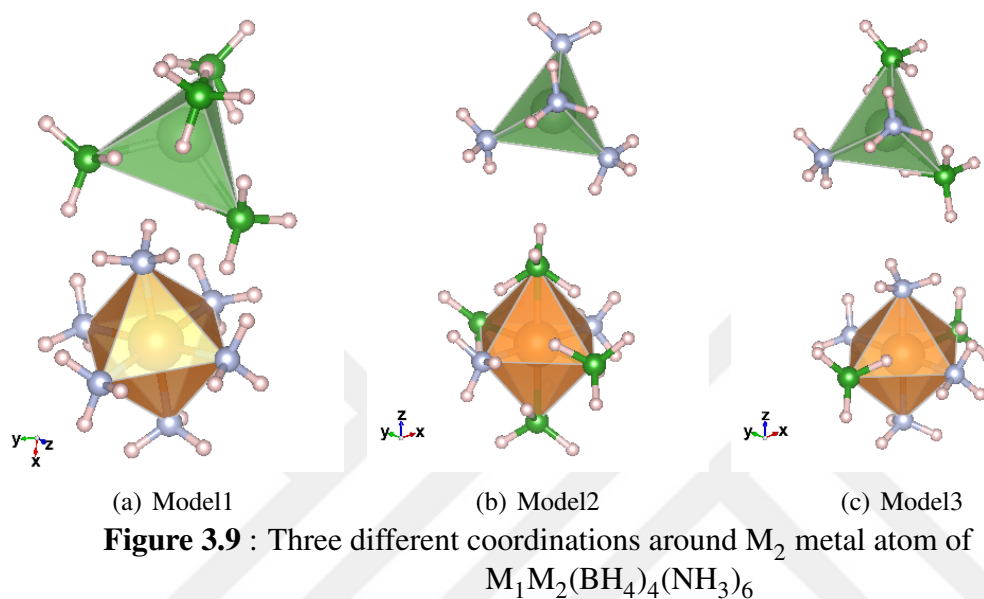
**Figure 3.8** :  $\text{M}_1\text{M}_2(\text{BH}_4)_4(\text{NH}_3)_5$  structures found by CASPESA

The template structures indicate major structural changes upon the DFT relaxations. In particular, B4N5\_1 prefers an octahedral arrangement consisting of five  $\text{NH}_3$  and one  $\text{BH}_4$  groups around  $\text{M}_2$ . In the case of  $\text{M}_1$ , a trigonal coordination including  $\text{BH}_4$  groups is present around  $\text{M}_1$ . In structure B4N5\_2,  $\text{M}_2$  metals are forming quite distorted octahedral coordinations while  $\text{M}_1$  prefers both tetrahedral and trigonal coordinations including  $\text{BH}_4$  groups. In B4N5\_3,  $\text{M}_1$  and  $\text{M}_2$  form tetrahedral and

octahedral arrangements respectively. Moreover,  $M_1$  metals are share two of their  $BH_4$  groups with each other.

### 3.1.5 Crystal structure predictions for $M_1M_2(BH_4)_4(NH_3)_6$

Three different models shown in figure 3.9 were employed for the inspection of  $M_1M_2(BH_4)_4(NH_3)_6$ .



In the first model, all of the  $BH_4$  and  $NH_3$  groups are located around  $M_1$  and  $M_2$  in a tetrahedral and octahedral fashion respectively. In the second model, two  $NH_3$  and four  $BH_4$  groups are positioned octahedrally around  $M_2$  and  $M_1$  is surrounded by a tetrahedral consisting of  $NH_3$  groups. The last model is a variant of Model2; binding positions of  $BH_4$  and  $NH_3$  groups to  $M_2$  is altered.

Three template structures shown in figure 3.10 were obtained after the DFT optimizations.

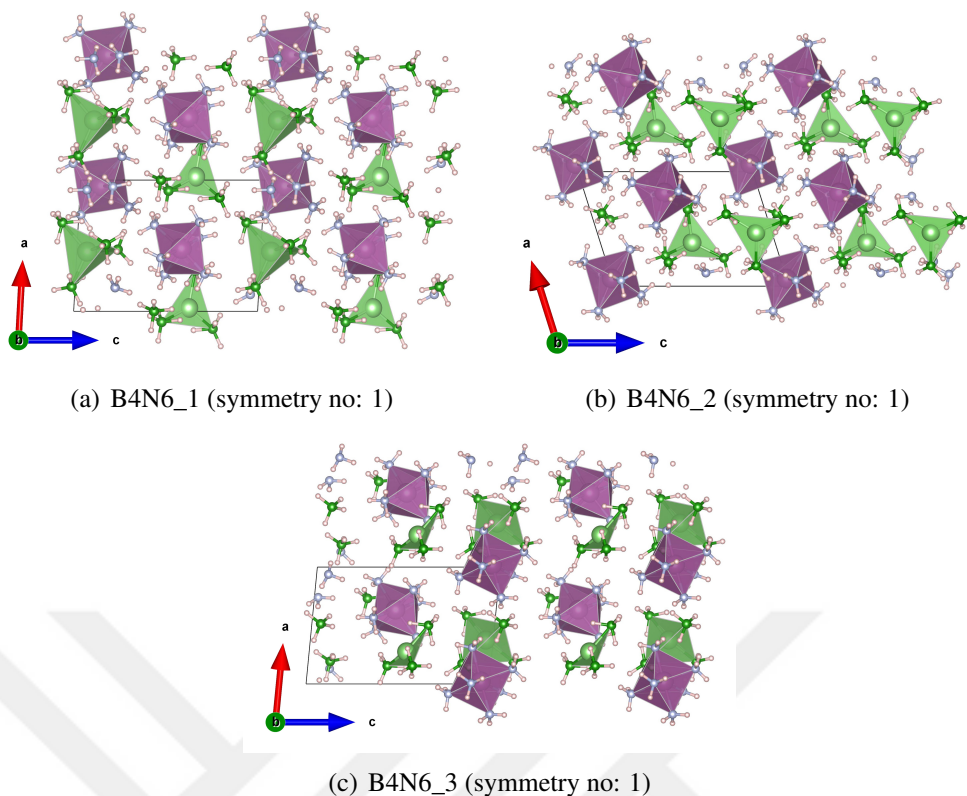


**Figure 3.10** :  $M_1M_2(BH_4)_4(NH_3)_6$  structures found by CASPESA

$M_2$  metal is surrounded by six  $NH_3$  groups in all template structures. While  $M_1$  metal forms both trigonal and tetrahedral coordinations in B4N6\_1 and B4N6\_3, there is only a tetrahedral in B4N6\_2.

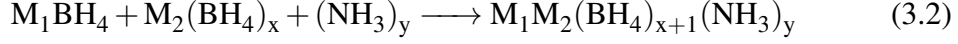
### 3.2 Computational Screening

In the screening of dual-cation AMBs with general formula of  $M_1M_2(BH_4)_4(NH_3)_{2-6}$ , Li, Na and K alkali metals were used as  $M_1$  and Al, Sc, Mo, Co, Y, Ti atoms were used as  $M_2$ . In order to find template structures, Li and Sc were employed as  $M_1$  and  $M_2$  respectively in the initial DFT calculations. Then, to find the energy of the other AMBs,  $M_1$  and  $M_2$  atoms were changed in the template structure and DFT calculations have been performed to optimize cell parameters and atomic positions. To assess the screening results a selection criteria similar to Hummelshøj et al. [7] (stability against to phase separation (alloying) and decomposition) were used. Three different reactions were considered as a phase separation. Among them, the first one is inspired from Soloveichik et al. [28]. They synthesized  $Mg(BH_4)_2(NH_3)_6$  according

to reaction shown below:



Dual cation AMBs can be obtained by adding an alkali metal borohydride to this reaction.



Based on the above reaction, an alloying energy can be calculated as below:

$$\Delta E_{\text{alloy1}} = E_{\text{M}_1\text{M}_2(\text{BH}_4)_{x+1}(\text{NH}_3)_y} - (E_{\text{M}_1\text{BH}_4} + E_{\text{M}_2(\text{BH}_4)_x} + yE_{\text{NH}_3}) \quad (3.3)$$

here,  $E_{\text{M}_1\text{M}_2(\text{BH}_4)_{x+1}(\text{NH}_3)_y}$  is energy of dual cation AMB,  $E_{\text{M}_1\text{BH}_4}$  is energy of alkali borohydride and  $E_{\text{M}_2(\text{BH}_4)_x}$  is the energy of the other metal borohydride. Recently, a  $\text{Li}_2\text{Mg}(\text{BH}_4)_4 \cdot 6\text{NH}_3$  were synthesized by Yang et al. [38] with following reaction:



This screening study also includes a general form of this reaction. In the literature  $\text{M}(\text{BH}_4)_2(\text{NH}_3)_2$  (M=Mg, Ca and Zn) [38] and  $\text{Mg}(\text{BH}_4)_2(\text{NH}_3)_6$  [28] are the only reported crystal structures for  $\text{M}(\text{BH}_4)_2(\text{NH}_3)_y$  (here M=M<sub>2</sub> atom). Accordingly, the above reaction was readjusted based on the known complexes. In the light of these informations, alloying energies are calculated as below:

$$\Delta E_{\text{alloy2}} = E_{\text{M}_1\text{M}_2(\text{BH}_4)_{x+1}(\text{NH}_3)_y} - (E_{\text{M}_1\text{BH}_4} + E_{\text{M}_2(\text{BH}_4)_x(\text{NH}_3)_y})$$

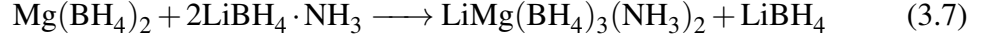
for  $y = 2$  and  $y = 6$  (3.5)

$$\Delta E_{\text{alloy2}} = E_{\text{M}_1\text{M}_2(\text{BH}_4)_{x+1}(\text{NH}_3)_y} - (E_{\text{M}_1\text{BH}_4} + E_{\text{M}_2(\text{BH}_4)_x(\text{NH}_3)_2} + (y-2)E_{\text{NH}_3})$$

for  $y = 3, 4, 5$  (3.6)

In order to calculate the energy of  $\text{M}(\text{BH}_4)_2(\text{NH}_3)_2$  (M=Al, Sc, Mo, Co, Y and Ti), the corresponding metal atoms in the experimental crystal structures of Mg, Ca and Zn were replaced with Al, Sc, Mo, Co, Y and Ti and then these systems were relaxed by DFT to obtain the lowest energy structure which subsequently invoked in the calculation of  $\Delta E_{\text{alloy2}}$ .

The last alloying reaction was inspired from the synthesis of  $\text{LiMg}(\text{BH}_4)_3(\text{NH}_3)_2$  [16] involving ball-milling of  $\text{LiBH}_4 \cdot \text{NH}_3$  and  $\text{Mg}(\text{BH}_4)_2$  as shown in the following equation.



$\Delta E_{\text{alloy3}}$  were calculated from the general form of this equation as below:

$$\Delta E_{\text{alloy3}} = (E_{\text{M}_1\text{M}_2(\text{BH}_4)_{x+1}(\text{NH}_3)_n} + (n-1)E_{\text{LiBH}_4}) - (E_{\text{M}_2(\text{BH}_4)_x} + nE_{\text{M}_1\text{BH}_4\text{NH}_3}) \quad (3.8)$$

The total energy of  $\text{M}_1\text{BH}_4\text{NH}_3$  must be known to calculate  $\Delta E_{\text{alloy3}}$ . Recently, Guo et al. [27] found that  $\text{LiBH}_4\text{NH}_3$  crystallizes in the orthorhombic structure ( $a=5.97$ ,  $b=4.64$  and  $c=14.35$  Å) with space group *Pnma* (IT number 62). Each Li atom in this structure has a tetrahedral coordination containing three  $\text{BH}_4$  and one  $\text{NH}_3$  molecules. Li atoms create a chain parallel to [010] direction by sharing two  $\text{BH}_4$  groups. There is no reported experimental structure concerning a  $\text{NaBH}_4\text{NH}_3$  and  $\text{KBH}_4\text{NH}_3$  in the literature. The calculation of the total energies regarding to these systems were done by swapping Li in  $\text{LiBH}_4\text{NH}_3$  with Na and K.

Similar to binary and ternary metal borohydrides [7], the decomposition pathways of dual cation AMBs are highly complex and produce different species such as metal hydrides, ammonia,  $\text{BN}_3$ ,  $\text{HBN}_2$ , diborane ( $\text{B}_2\text{H}_6$ ) and borazine ( $(\text{HBNH})_3$ ). When the fact that a very limited knowledge about the true decomposition pathways of AMBs is present and the scope of this screening study are considered together, the best option is to select a generic decomposition pathway as the evaluation criterion. In this respect, the first generic pathway was designed by mimicking the decomposition of  $\text{Li}_2\text{Mg}(\text{BH}_4)_4(\text{NH}_3)_6$  [34]. Yang et al. [34] observed that this complex decomposes by following three stages: i) at  $195^\circ\text{C}$   $\text{Li}_2\text{Mg}(\text{BH}_4)_4(\text{NH}_3)_3$  appears together with ammonia release, ii) at  $270^\circ\text{C}$   $\text{Li}_2\text{Mg}(\text{BH}_4)_4(\text{NH}_3)_3$  disappears and  $\text{LiBH}_4$  and  $\text{MgB}_2\text{N}_3$  form in addition to hydrogen and ammonia, iii) an increase of the decomposition temperature to  $450^\circ\text{C}$  forms Mg, BN, LiH, B and ammonia and hydrogen gases. A generalized version of the last step of this decomposition reaction was employed in our screening and the corresponding decomposition energy

( $\Delta E_{decomp1}$ ) can be calculated as shown below:

$$\begin{aligned} \Delta E_{decomp1} = & E_{M_1M_2(BH_4)_x(NH_3)_y} - (E_{M_1H} + E_{M_2} + \frac{y}{2}E_{NH_3} + \frac{y}{2}E_{BN} \\ & + (x - \frac{y}{2})E_B + ((3y + 5x) - (\frac{3y}{2} + 1))E_{H_2} \end{aligned} \quad (3.9)$$

Recently, Xia et al. [17] reported the synthesis and dehydrogenation performance of  $NaZn(BH_4)_3(NH_3)_2$ . Their decomposition experiments revealed that at 200 °C  $NaBH_4$ ,  $NH_3$ ,  $BN$ ,  $Zn$  and hydrogen are formed. This reaction is the second decomposition pathway employed in the screening study and the corresponding decomposition energy ( $\Delta E_{decomp2}$ ) can be obtained as follows:

$$\begin{aligned} \Delta E_{decomp2} = & E_{M_1M_2(BH_4)_x(NH_3)_y} - (E_{M_2} + E_{M_1BH_4} + (x - 1)E_{BN} \\ & + (y - x + 1)E_{NH_3} + (\frac{7x}{2} + \frac{7}{2})E_{H_2}) \end{aligned} \quad (3.10)$$

Both alloying and decomposition energy equations require the computation of additional energy terms ( $E_{M_1BH_4}$ ,  $E_{M_2(BH_4)_2}$ ,  $E_{NH_3}$ ,  $E_{M_1H}$ ,  $E_{BN}$ ,  $E_B$ ,  $E_{M_2}$  and  $E_{H_2}$ ) as well as the energy of AMBs. Among them, the energies of  $H_2$  and  $NH_3$  were obtained by putting them in a cubic cell with a dimension of 10Å.  $\alpha$ -rhombohedral boron containing icosahedrons was used for the calculation of  $E_B$ . While a face-centered cubic cell was used for Ca, Sr and Ni, a base-centered cubic cell was utilized for Li, Na, K and Mn. For the remaining metals (Mg and Zn), a hexagonal close-packed cell was employed. All of the alkali metal hydrides ( $LiH$ ,  $NaH$  and  $KH$ ) crystallize in the form of  $NaCl$  with  $Fm-3m$  space group. The crystal structures of most of the metal borohydrides were taken from the literature. For instance, an orthorhombic structure with space group  $I4m2$  (IT 119) found by Tekin et al. [19] was employed for  $LiBH_4$ . The tetragonal structures with space group  $P4_2/nmc$  (IT 137) and  $I4m2$  (IT 119) reported in Caputo et al. [20, 21] were used respectively for  $NaBH_4$  and  $Mg(BH_4)_2$ . It has been found that  $KBH_4$  crystallizes in a tetragonal structure with space group  $P4_2/nmc$  (IT 137) [39, 40] and this structure was considered in the screening. All the remaining details of these structures are listed in Table 2.1.

For the evaluation of the screening, similar to Hummelshoj et al. [7], two criteria were employed: i) the alloying energy must be lower than zero and ii)  $-0.8 \leq \Delta E_{decomp} \leq 0.0$  eV/ $H_2$ . The employed decomposition energy range (0.2 – 0.8 eV) is accepted as the ideal energy range in the literature [47, 48].



**Table 3.1** : Cell parameters of structures which are used in the screening.

Metal	a	b	c	$\alpha$	$\beta$	$\gamma$	Symmetry	Reference
Li	3.44						$Pm\bar{3}m(221)$	
Na	4.23						$Pm\bar{3}m(221)$	
K	5.16						$Pm\bar{3}m(221)$	
Ca	5.53						$Pm\bar{3}m(221)$	
Sr	5.94						$Pm\bar{3}m(221)$	
Ni	3.54						$Pm\bar{3}m(221)$	
Mn	8.74						$P\bar{4}3m(215)$	
Mg	3.83	3.83	4.03	90	90	120	$P6_3/mmc(194)$	
Zn	3.20	3.20	3.41	90	90	120	$P6_3/mmc(194)$	
B	4.89	4.89	12.44	90	90	120	$R\bar{3}m(166)$	
Co	3.20	3.77	3.81	90	90	90	$Cmcm(63)$	
Mo	3.16	3.16	3.16	90	90	90	$Pm\bar{3}m(221)$	
Ti	2.36	2.36	6.23	90	90	120	$P6_3/mmc(194)$	
Zr	2.58	2.58	6.77	90	90	120	$P6_3/mmc(194)$	
LiH	4.04						$Fm\bar{3}m(225)$	
NaH	4.80						$Fm\bar{3}m(225)$	
KH	5.46						$Fm\bar{3}m(225)$	
LiBH <sub>4</sub>	8.48	4.35	5.75	90	90	90	$Pnma(62)$	[19]
NaBH <sub>4</sub>	4.36	4.36	5.90	90	90	90	$P4_2/nmc(137)$	[21]
KBH <sub>4</sub>	4.75	4.75	6.66	90	90	90	$P4_2/nmc(137)$	[39]
Ca(BH <sub>4</sub> ) <sub>2</sub>	8.79	13.14	7.50	90	90	90	$Fddd(70)$	[41]
Sr(BH <sub>4</sub> ) <sub>2</sub>	7.02	8.51	7.62	90	90	90	$Pbcn(60)$	[42]
Ni(BH <sub>4</sub> ) <sub>2</sub>	7.23	7.23	10.05	88.24	91.79	87.04	$P1(1)$	[19]
Mn(BH <sub>4</sub> ) <sub>2</sub>	10.43	10.43	10.83	90	90	90	$P3_112(151)$	[43]
Mg(BH <sub>4</sub> ) <sub>2</sub>	8.18	8.18	10.07	90	90	90	$I\bar{4}m2(119)$	[19]
Zn(BH <sub>4</sub> ) <sub>2</sub>	4.12	4.86	7.92	90	90	90	$Pmc2_1(26)$	[44]
Zn(BH <sub>4</sub> ) <sub>2</sub>	9.93	11.18	11.89	90	90	90	$F222(22)$	[44]
Zn(BH <sub>4</sub> ) <sub>2</sub>	8.30	8.30	9.34	90	90	90	$I\bar{4}m2(119)$	[44]
Zn(BH <sub>4</sub> ) <sub>2</sub>	6.99	6.99	12.19	90	90	90	$I4_122(98)$	[44]
Zn(BH <sub>4</sub> ) <sub>2</sub>	6.88	5.44	7.84	89.50	76.15	89.98	$P\bar{1}(2)$	[44]
Co(BH <sub>4</sub> ) <sub>3</sub>	34.48	11.78	12.05	90	90	90	$Pna2_1(33)$	[12]
Mo(BH <sub>4</sub> ) <sub>3</sub>	6.93	12.14	8.67	90	90	90	$P2_12_12(18)$	[45]
Ti(BH <sub>4</sub> ) <sub>3</sub>	8.85	12.56	7.17	90	90	90	$P222_1(17)$	[45]
Co(BH <sub>4</sub> ) <sub>4</sub>	5.71						$P\bar{4}3m(215)$	[46]
Mn(BH <sub>4</sub> ) <sub>4</sub>	6.02						$P\bar{4}3m(215)$	[46]
Mo(BH <sub>4</sub> ) <sub>4</sub>	6.20						$P\bar{4}3m(215)$	[46]
Ti(BH <sub>4</sub> ) <sub>4</sub>	6.10						$P\bar{4}3m(215)$	[46]
Zr(BH <sub>4</sub> ) <sub>4</sub>	6.34						$P\bar{4}3m(215)$	[46]
BN	2.53	2.53	6.96	90	90	120	$P6_3/mmc(194)$	[44]
LiBH <sub>4</sub> NH <sub>3</sub>	6.13	4.39	13.41	90	90	90	$Pnma(62)$	[27]
NaBH <sub>4</sub> NH <sub>3</sub>	6.42	4.72	14.54	90	90	90	$Pnma(62)$	[27]
KBH <sub>4</sub> NH <sub>3</sub>	6.83	5.03	14.83	90	90	90	$Pnma(62)$	[27]

### 3.2.1 Screening results for $M_1M_2(BH_4)_4(NH_3)_y$

$\Delta E_{alloy1}$  and  $\Delta E_{alloy3}$  were generally obtained to be negative (and close to each other). This indicates that most of the alloys are stable against separation for the investigated 90 dual-cation AMBs. On the other hand,  $\Delta E_{alloy2}$  was calculated to be positive for more than half of considered alloys. Seeing that  $\Delta E_{alloy3}$  is the most artificial alloying energy, it has been excluded from the screening. The decomposition energies ( $\Delta E_{decomp1}$  and  $\Delta E_{decomp2}$ ) were mostly negative and they were in the following ranges (-0.777,-0.231) and (-0.707,-0.088), respectively. The alloying energy ( $\Delta E_{alloy1}$ ) was plotted against the decomposition energies ( $\Delta E_{decomp1}$  and  $\Delta E_{decomp2}$ ) in figure 3.11 and figure 3.12 respectively.

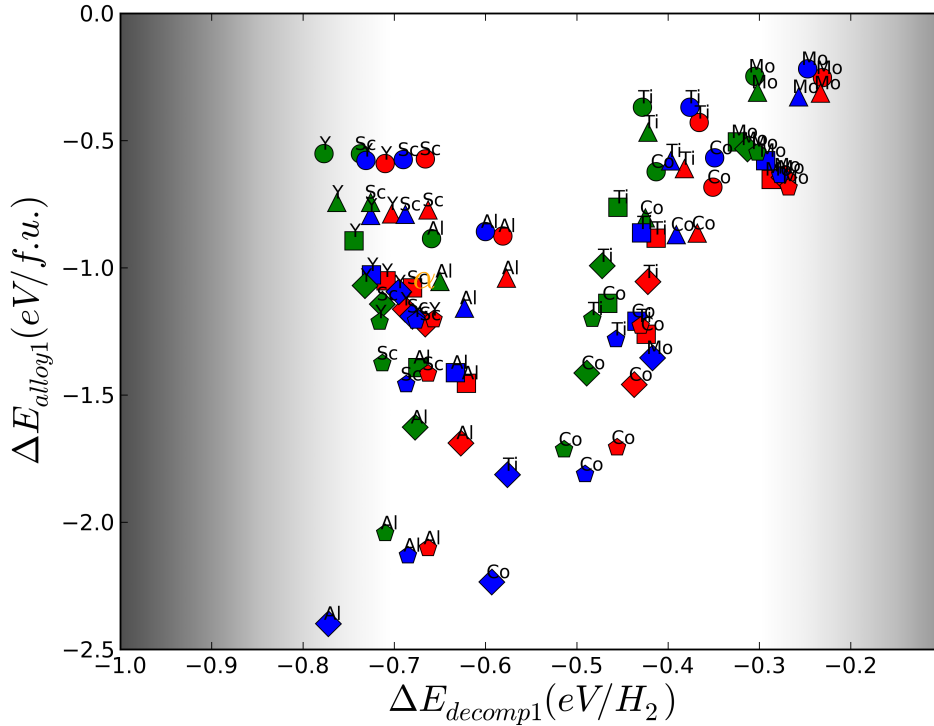


**Figure 3.11** : The alloying energy,  $\Delta E_{alloy1}$ , as function of the decomposition energy,  $\Delta E_{decomp1}$ . Representative colors: Li (Red), Na (Blue), K (Green). NH<sub>3</sub> content: x=2 (circle), x=3 (triangle), x=4 (square), x=5 (diamond) and x=6 (pentagon).

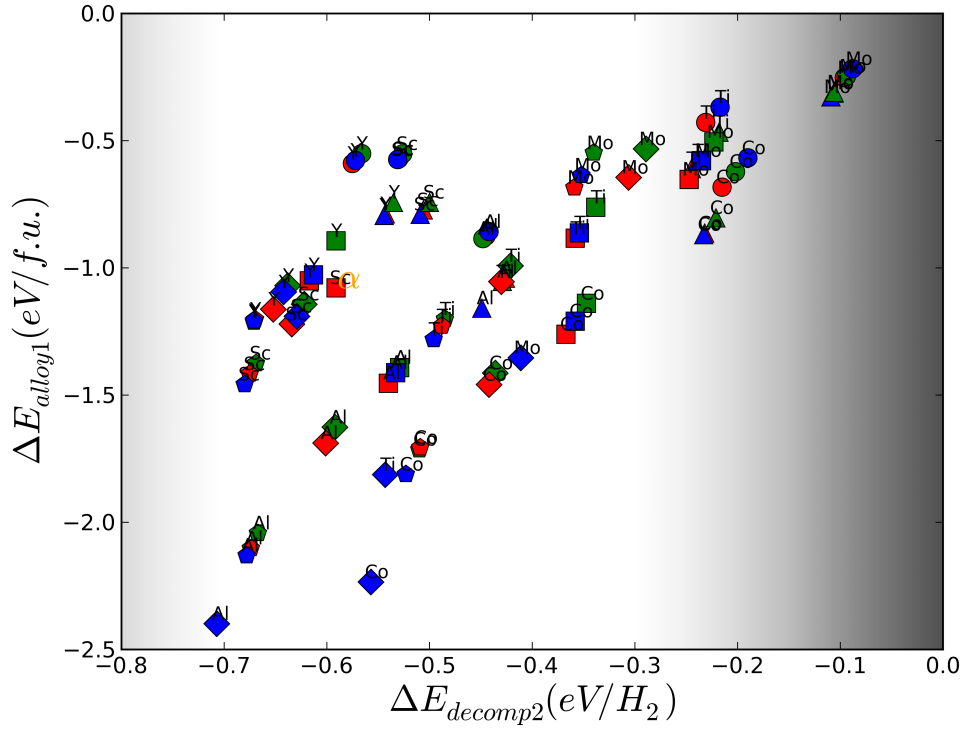


**Figure 3.12 :** The alloying energy,  $\Delta E_{alloy1}$ , as function of the decomposition energy,  $\Delta E_{decomp2}$ . Representative colors: Li (Red), Na (Blue), K (Green).  $NH_3$  content: x=2 (circle), x=3 (triangle), x=4 (square), x=5 (diamond) and x=6 (pentagon).

It is clear from these figures that almost all of the considered alloys are in the desired region. Among these alloys the only synthesized one,  $LiSc(BH_4)_4(NH_3)_4$  [42] and it is also found in the desired region. In general,  $\Delta E_{decomp1}$  is more negative than  $\Delta E_{decomp2}$ . In the case of alloying energies,  $\Delta E_{alloy1}$  was obtained more negative. The calculated values for the experimentally synthesized  $LiSc(BH_4)_4(NH_3)_4$  is as follows:  $\Delta E_{alloy1} = -1.079$  eV,  $\Delta E_{decomp1} = -0.680$  eV,  $\Delta E_{decomp2} = -0.591$  eV. The amount of stored hydrogen in these alloys is depicted in figure 3.13 and 3.14 as a function of decomposition energies.

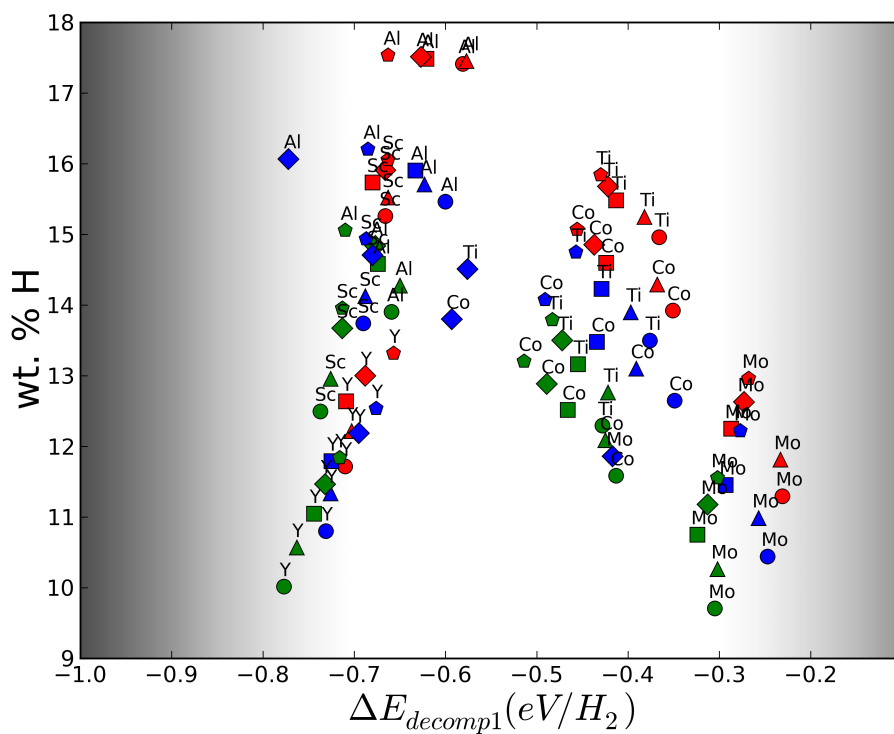


**Figure 3.13 :** Hydrogen capacity (wt %) as a function of the decomposition energy,  $\Delta E_{decomp1}$ . Representative colors: Li (Red), Na (Blue), K (Green).  $NH_3$  content: x=2 (circle), x=3 (triangle), x=4 (square), x=5 (diamond) and x=6 (pentagon).

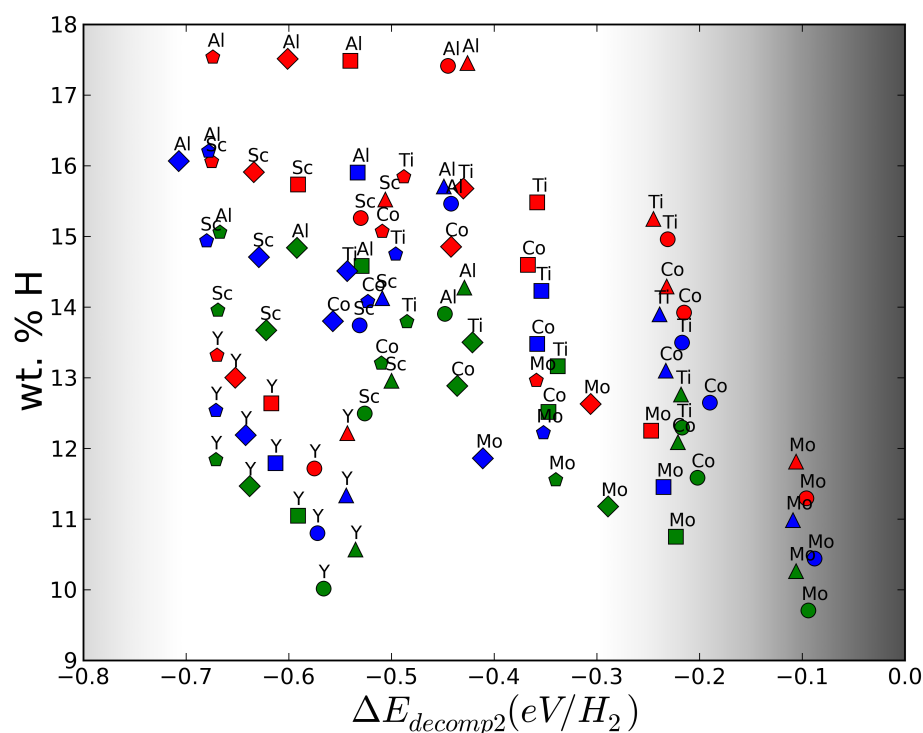


**Figure 3.14** : Hydrogen capacity (wt %) as a function of the decomposition energy,  $\Delta E_{decomp2}$ . Representative colors: Li (Red), Na (Blue), K (Green).  $\text{NH}_3$  content: x=2 (circle), x=3 (triangle), x=4 (square), x=5 (diamond) and x=6 (pentagon).

It is apparent from these figures that all of the concerned alloys have storage capacity above the DOE 2025 target of 5.5 wt %. Among the alloys, the ones containing LiAl (up to 17.533 wt %) have the highest hydrogen storage capacity.

It has been showed that there is a linear correlation between the decomposition temperature and the average cation Pauling electronegativity [7]. Average Pauling electronegativity as a function of decomposition energy ( $\Delta E_{alloy1}$ ) can be seen in the figure 3.15.

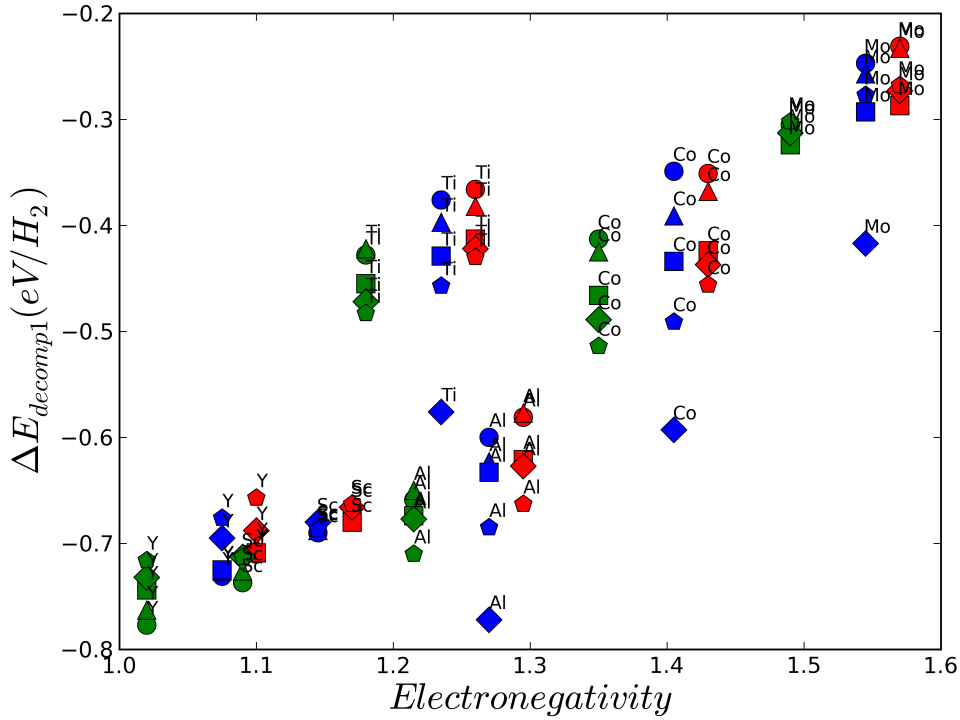


**Figure 3.15** : The decomposition energy,  $\Delta E_{decomp1}$ , as a function of the average Pauling electronegativity. Representative colors: Li (Red), Na (Blue), K (Green).  $\text{NH}_3$  content:  $x=2$  (circle),  $x=3$  (triangle),  $x=4$  (square),  $x=5$  (diamond) and  $x=6$  (pentagon).

As can be seen from the figure, the linear correlation is only violated by the alloys containing Ti. Similar to the screening study of Hummelshoj et al. [7], the most promising alloys have electronegativities around 1.1 - 1.4. Lastly, alloys containing Y and Sc have the smallest electronegativity values while alloys containing Mo have the highest values.

### 3.3 Conclusions

The first approach of our screening study was predicting crystal structures since huge amount of crystal structure details of dual cation AMBs are unknown. In the screened system,  $\text{M}_1\text{M}_2(\text{BH}_4)_4(\text{NH}_3)_x$ ,  $\text{LiSc}(\text{BH}_4)_4(\text{NH}_3)_4$  is the only experimentally synthesized system and it was found to be in desired region of our screening study. The developed crystal structure prediction algorithm, CASPESA, was successfully applied for all the systems. Before anything else, CASPESA predicted fairly similar structures to  $\text{LiSc}(\text{BH}_4)_4(\text{NH}_3)_4$ . Furthermore, CASPESA was also generated promising crystal structures concerning to remaining systems. Among the inspected materials alloys

containing Al with Li have the highest hydrogen content. In addition, alloys containing Li with Sc, Li with Ti and Na with Al have fair amount of hydrogen content. In case of decomposition and alloying energies of the screened materials, alloys containing Li, Na, K with Mo,Co (while  $x < 6$  and except  $\text{NaCo}(\text{BH}_4)_4(\text{NH}_3)_4$ ), Ti (except  $\text{NaTi}(\text{BH}_4)_4(\text{NH}_3)_4$ ) and Al (while  $x < 5$ ) estimated to be more favourable. To sum up, the only experimentally synthesized complex,  $\text{LiSc}(\text{BH}_4)_4(\text{NH}_3)_4$ , reside in the desired region and screening results show a lot of promising materials which have not been synthesized yet.







## REFERENCES

- [1] **Smil, V.** (2000). Energy in the twentieth century: resources, conversions, costs, uses, and consequences, *Annual Review of Energy and the Environment*, 25(1), 21–51.
- [2] **Schlapbach, L. and Züttel, A.** (2001). Hydrogen-storage materials for mobile applications, *Nature*, 414(6861), 353–358.
- [3] **Züttel, A.** (2003). Materials for hydrogen storage, *Materials today*, 6(9), 24–33.
- [4] **Andreasen, A., Sørensen, M., Burkarl, R., Møller, B., Molenbroek, A., Pedersen, A., Vegge, T. and Jensen, T.R.** (2006). Dehydrogenation kinetics of air-exposed MgH<sub>2</sub>/Mg<sub>2</sub>Cu and MgH<sub>2</sub>/MgCu<sub>2</sub> studied with in situ X-ray powder diffraction, *Applied Physics A*, 82(3), 515–521.
- [5] **Lee, S.M. and Lee, Y.H.** (2000). Hydrogen storage in single-walled carbon nanotubes, *Applied Physics Letters*, 76(20), 2877–2879.
- [6] **Liu, Y., Kabbour, H., Brown, C.M., Neumann, D.A. and Ahn, C.C.** (2008). Increasing the density of adsorbed hydrogen with coordinatively unsaturated metal centers in metal-organic frameworks, *Langmuir*, 24(9), 4772–4777.
- [7] **Hummelshøj, J.S., Landis, D., Voss, J., Jiang, T., Tekin, A., Bork, N., Duřak, M., Mortensen, J.J., Adamska, L., Andersin, J. et al.** (2009). Density functional theory based screening of ternary alkali-transition metal borohydrides: A computational material design project, *The Journal of chemical physics*, 131(1), 014101.
- [8] **Rude, L.H., Nielsen, T.K., Ravensbaek, D.B., Boesenberg, U., Ley, M.B., Richter, B., Arnbjerg, L.M., Dornheim, M., Filinchuk, Y., Besenbacher, F. et al.** (2011). Tailoring properties of borohydrides for hydrogen storage: a review, *physica status solidi (a)*, 208(8), 1754–1773.
- [9] **Feaver, A., Sepehri, S., Shamberger, P., Stowe, A., Autrey, T. and Cao, G.** (2007). Coherent carbon cryogel-ammonia borane nanocomposites for H<sub>2</sub> storage, *The Journal of Physical Chemistry B*, 111(26), 7469–7472.
- [10] **Lohstroh, W. and Fichtner, M.** (2007). Reaction steps in the Li–Mg–N–H hydrogen storage system, *Journal of Alloys and Compounds*, 446, 332–335.
- [11] **Frankcombe, T.J., Kroes, G.J. and Züttel, A.** (2005). Theoretical calculation of the energy of formation of LiBH<sub>4</sub>, *Chemical physics letters*, 405(1), 73–78.

- [12] **Miwa, K., Ohba, N., Towata, S.i., Nakamori, Y., Züttel, A. and Orimo, S.i.** (2007). First-principles study on thermodynamical stability of metal borohydrides: Aluminum borohydride  $\text{Al}(\text{BH}_4)_3$ , *Journal of Alloys and Compounds*, 446, 310–314.
- [13] **Guo, Y., Yu, X., Sun, W., Sun, D. and Yang, W.** (2011). The Hydrogen-Enriched Al–B–N System as an Advanced Solid Hydrogen-Storage Candidate, *Angewandte Chemie*, 123(5), 1119–1123.
- [14] **Chu, H., Wu, G., Xiong, Z., Guo, J., He, T. and Chen, P.** (2010). Structure and hydrogen storage properties of calcium borohydride diammoniate, *Chemistry of Materials*, 22(21), 6021–6028.
- [15] **Guo, Y., Xia, G., Zhu, Y., Gao, L. and Yu, X.** (2010). Hydrogen release from amminelithium borohydride,  $\text{LiBH}_4 \cdot \text{NH}_3$ , *Chemical Communications*, 46(15), 2599–2601.
- [16] **Sun, W., Chen, X., Gu, Q., Wallwork, K.S., Tan, Y., Tang, Z. and Yu, X.** (2012). A New Ammine Dual-Cation (Li, Mg) Borohydride: Synthesis, Structure, and Dehydrogenation Enhancement, *Chemistry–A European Journal*, 18(22), 6825–6834.
- [17] **Xia, G., Gu, Q., Guo, Y. and Yu, X.** (2012). Ammine bimetallic (Na, Zn) borohydride for advanced chemical hydrogen storage, *Journal of Materials Chemistry*, 22(15), 7300–7307.
- [18] **Guo, Y., Wu, H., Zhou, W. and Yu, X.** (2011). Dehydrogenation tuning of ammine borohydrides using double-metal cations, *Journal of the American Chemical Society*, 133(13), 4690–4693.
- [19] **Tekin, A., Caputo, R. and Züttel, A.** (2010). First-principles determination of the ground-state structure of  $\text{LiBH}_4$ , *Physical review letters*, 104(21), 215501.
- [20] **Caputo, R., Tekin, A., Sikora, W. and Züttel, A.** (2009). First-principles determination of the ground-state structure of  $\text{Mg}(\text{BH}_4)_2$ , *Chemical Physics Letters*, 480(4), 203–209.
- [21] **Caputo, R. and Tekin, A.** (2011). Ab-initio crystal structure prediction. A case study:  $\text{NaBH}_4$ , *Journal of solid state chemistry*, 184(7), 1622–1630.
- [22] **Caputo, R. and Tekin, A.** (2012). Lithium dihydroborate: first-principles structure prediction of  $\text{LiBH}_2$ , *Inorganic chemistry*, 51(18), 9757–9765.
- [23] **Caputo, R., Kupczak, A., Sikora, W. and Tekin, A.** (2013). Ab initio crystal structure prediction by combining symmetry analysis representations and total energy calculations. An insight into the structure of  $\text{Mg}(\text{BH}_4)_2$ , *Physical Chemistry Chemical Physics*, 15(5), 1471–1480.
- [24] **Tekin, A., Hummelshøj, J.S., Jacobsen, H.S., Sveinbjörnsson, D., Blanchard, D., Nørskov, J.K. and Vegge, T.** (2010). Ammonia dynamics in magnesium ammine from DFT and neutron scattering, *Energy & Environmental Science*, 3(4), 448–456.

- [25] Churchard, A.J., Banach, E., Borgschulte, A., Caputo, R., Chen, J.C., Clary, D., Fijalkowski, K.J., Geerlings, H., Genova, R.V., Grochala, W. *et al.* (2011). A multifaceted approach to hydrogen storage, *Physical Chemistry Chemical Physics*, 13(38), 16955–16972.
- [26] Aftandilian, V., Miller, H. and Muetterties, E. (1961). Chemistry of boranes. I. Reactions of boron hydrides with metal and amine salts, *Journal of the American Chemical Society*, 83(11), 2471–2474.
- [27] Guo, Y., Jiang, Y., Xia, G. and Yu, X. (2012). Ammine aluminium borohydrides: an appealing system releasing over 12 wt% pure H<sub>2</sub> under moderate temperature, *Chemical Communications*, 48(37), 4408–4410.
- [28] Soloveichik, G., Her, J.H., Stephens, P.W., Gao, Y., Rijssenbeek, J., Andrus, M. and Zhao, J.C. (2008). Ammine magnesium borohydride complex as a new material for hydrogen storage: structure and properties of Mg (BH<sub>4</sub>)<sub>2</sub> · 2NH<sub>3</sub>, *Inorganic chemistry*, 47(10), 4290–4298.
- [29] Tang, Z., Tan, Y., Gu, Q. and Yu, X. (2012). A novel aided-cation strategy to advance the dehydrogenation of calcium borohydride monoammoniate, *Journal of Materials Chemistry*, 22(12), 5312–5318.
- [30] Yuan, F., Gu, Q., Guo, Y., Sun, W., Chen, X. and Yu, X. (2012). Structure and hydrogen storage properties of the first rare-earth metal borohydride ammoniate: Y (BH<sub>4</sub>)<sub>3</sub> · 4NH<sub>3</sub>, *Journal of Materials Chemistry*, 22(3), 1061–1068.
- [31] Yuan, F., Gu, Q., Chen, X., Tan, Y., Guo, Y. and Yu, X. (2012). Complex ammine titanium (III) borohydrides as advanced solid hydrogen-storage materials with favorable dehydrogenation properties, *Chemistry of Materials*, 24(17), 3370–3379.
- [32] Gu, Q., Gao, L., Guo, Y., Tan, Y., Tang, Z., Wallwork, K.S., Zhang, F. and Yu, X. (2012). Structure and decomposition of zinc borohydride ammonia adduct: towards a pure hydrogen release, *Energy & Environmental Science*, 5(6), 7590–7600.
- [33] Hagemann, H., Longhini, M., Kaminski, J.W., Wesolowski, T.A., Cerny, R., Penin, N., Sørby, M.H., Hauback, B.C., Severa, G. and Jensen, C.M. (2008). LiSc (BH<sub>4</sub>)<sub>4</sub>: a novel salt of Li<sup>+</sup> and discrete Sc (BH<sub>4</sub>)<sub>4</sub><sup>-</sup> complex anions, *The Journal of Physical Chemistry A*, 112(33), 7551–7555.
- [34] Yang, Y., Liu, Y., Wu, H., Zhou, W., Gao, M. and Pan, H. (2014). An ammonia-stabilized mixed-cation borohydride: synthesis, structure and thermal decomposition behavior, *Physical Chemistry Chemical Physics*, 16(1), 135–143.
- [35] Giannozzi, P., Baroni, S., Bonini, N., Calandra, M., Car, R., Cavazzoni, C., Ceresoli, D., Chiarotti, G.L., Cococcioni, M., Dabo, I. *et al.* (2009). QUANTUM ESPRESSO: a modular and open-source software project for quantum simulations of materials, *Journal of Physics: Condensed Matter*, 21(39), 395502.

- [36] Perdew, J.P., Burke, K. and Ernzerhof, M. (1996). Generalized gradient approximation made simple, *Physical review letters*, 77(18), 3865.
- [37] Hohenberg, P. and Kohn, W. (1964). Inhomogeneous electron gas, *Physical review*, 136(3B), B864.
- [38] Chen, X. and Yu, X. (2012). Electronic structure and initial dehydrogenation mechanism of  $M(BH_4)_2 \cdot 2NH_3$  ( $M = Mg, Ca, \text{ and } Zn$ ): a first-principles investigation, *The Journal of Physical Chemistry C*, 116(22), 11900–11906.
- [39] Nakamori, Y., Miwa, K., Ninomiya, A., Li, H., Ohba, N., Towata, S.i., Züttel, A. and Orimo, S.i. (2006). Correlation between thermodynamical stabilities of metal borohydrides and cation electronegativities: First-principles calculations and experiments, *Physical Review B*, 74(4), 045126.
- [40] Renaudin, G., Gomes, S., Hagemann, H., Keller, L. and Yvon, K. (2004). Structural and spectroscopic studies on the alkali borohydrides  $MBH_4$  ( $M = Na, K, Rb, Cs$ ), *Journal of alloys and compounds*, 375(1), 98–106.
- [41] Miwa, K., Aoki, M., Noritake, T., Ohba, N., Nakamori, Y., Towata, S.i., Züttel, A. and Orimo, S.i. (2006). Thermodynamical stability of calcium borohydride  $Ca(BH_4)_2$ , *Physical Review B*, 74(15), 155122.
- [42] Ravnsbæk, D., Nickels, E., Cerny, R., Olesen, C., David, W., Edwards, P., Filinchuk, Y. and Jensen, T. (2013). Novel alkali earth borohydride  $Sr(BH_4)_2$  and borohydride-chloride  $Sr(BH_4)Cl$ , *Inorganic chemistry*, 52(19), 10877–10885.
- [43] Cerny, R., Penin, N., Hagemann, H. and Filinchuk, Y. (2009). The first crystallographic and spectroscopic characterization of a 3 d-metal borohydride:  $Mn(BH_4)_2$ , *The Journal of Physical Chemistry C*, 113(20), 9003–9007.
- [44] Kurakevych, O.O. and Solozhenko, V.L. (2007). Rhombohedral boron subnitride,  $B_13N_2$ , by X-ray powder diffraction, *Acta Crystallographica Section C: Crystal Structure Communications*, 63(9), i80–i82.
- [45] Kim, C., Hwang, S.J., Bowman Jr, R.C., Reiter, J.W., Zan, J.A., Kulleck, J.G., Kabbour, H., Majzoub, E. and Ozolins, V. (2009).  $LiSc(BH_4)_4$  as a hydrogen storage material: multinuclear high-Resolution solid-state NMR and first-Principles Density functional Theory Studies, *The Journal of Physical Chemistry C*, 113(22), 9956–9968.
- [46] Rude, L.H., Corno, M., Ugliengo, P., Baricco, M., Lee, Y.S., Cho, Y.W., Besenbacher, F., Overgaard, J. and Jensen, T.R. (2012). Synthesis and structural investigation of  $Zr(BH_4)_4$ , *The Journal of Physical Chemistry C*, 116(38), 20239–20245.
- [47] Walker, G. (2008). *Solid-state hydrogen storage: materials and chemistry*, Elsevier.

- [48] **Cobian, M. and Íñiguez, J.** (2008). Theoretical investigation of hydrogen storage in metal-intercalated graphitic materials, *Journal of Physics: Condensed Matter*, 20(28), 285212.





## CURRICULUM VITAE



**Name Surname:** Samet DEMIR

**Place and Date of Birth:** Sinop - 1988

**Address:** Sanayi mah. Sultan Selim cad. Boz sok. No:9/10 Kagithane Istanbul

**E-Mail:** sametdemir@gmail.com

**B.Sc.:** Istanbul Technical University - Applied Physics

**M.Sc.:** Istanbul Technical University - Computational Science and Engineering

### Professional Experience and Rewards:

- The PRACEdays16 Best Poster Award with the poster entitled “*Computational design of hydrogen storage materials*”

### List of Publications and Patents:

- Emdadi A., **Demir S.**, Kislak Y. and Tekin A., 2016: Computational Screening of Dual Cation Metal Ammine Borohydrides by Density Functional Theory *The Journal of Physical Chemistry*, (in revision)
- **Demir S.**, Y. Kışlak, A. Emdadi, A. Tekin, Computational design of new dual cation ammine metal borohydrides 4. *National High Performance Computing Conference*, 1-2 October, 2015, ODTÜ, Ankara (Turkey). (Talk)
- **Demir S.**, A. Tekin, Computational discovery of new dual cation metal ammine borohydrides *The Energy and Materials Research Conference (EMR 2015)*, 25-27 February, 2015, Madrid-Spain. (Talk)
- **Demir S.** and Tekin, A., 2015. Discovery of New Dual Cation Metal Ammine Borohydrides: A Computational Study. In *2nd International Congress on Energy Efficiency and Energy Related Materials (ENEFM2014)*, (pp. 413-419). Springer International Publishing.
- Emdadi, A., Kışlak, Y., **Demir S.** and Tekin, A., 2015. Computational Screening of Dual Cation Metal Ammine Borohydrides. In *2nd International Congress on Energy Efficiency and Energy Related Materials (ENEFM2014)*, (pp. 581-586). Springer International Publishing.